HHS Public Access

Author manuscript

Cell. Author manuscript; available in PMC 2019 July 26.

Published in final edited form as:

Cell. 2018 July 26; 174(3): 536–548.e21. doi:10.1016/j.cell.2018.06.004.

Defects in the alternative splicing-dependent regulation of REST cause deafness

Yoko Nakano[1,2], **Michael C. Kelly**[#3], **Atteeq U. Rehman**[#4,5], **Erich T. Boger**[6], **Robert J. Morell**[6], **Matthew W. Kelley**[3], **Thomas B. Friedman**[4], and **Botond Bánfi**[1,2,7,8,10,*]

[1]Department of Anatomy and Cell Biology, Carver College of Medicine, University of Iowa, Iowa City, IA 52242, USA

[2]Inflammation Program, Carver College of Medicine, University of Iowa, Iowa City, IA 52242, USA

[3]Laboratory of Cochlear Development, National Institute on Deafness and Other Communication Disorders, National Institutes of Health, Bethesda, MD 20892, USA

[4]Laboratory of Molecular Genetics, National Institute on Deafness and Other Communication Disorders, National Institutes of Health, Bethesda, MD 20892, USA

[5]Department of Molecular and Human Genetics, Baylor College of Medicine, Houston, TX 77030, USA

[6]Genomics and Computational Biology Core, National Institute on Deafness and Other Communication Disorders, National Institutes of Health, Bethesda, MD 20892, USA

[7]Department of Otolaryngology – Head and Neck Surgery, Carver College of Medicine, University of Iowa, Iowa City, IA 52242, USA

[8]Department of Internal Medicine, Carver College of Medicine, University of Iowa, Iowa City, IA 52242, USA

[10]Lead Contact

[#] These authors contributed equally to this work.

SUMMARY

The DNA-binding protein REST forms complexes with histone deacetylases (HDACs) to repress neuronal genes in non-neuronal cells. In differentiating neurons, REST is downregulated predominantly by transcriptional silencing. Here we report that post-transcriptional inactivation of REST by alternative splicing is required for hearing in humans and mice. We show that, in the mechanosensory hair cells of the mouse ear, regulated alternative splicing of a frameshift-causing

[*]Correspondence: botond-banfi@uiowa.edu.

AUTHOR CONTRIBUTIONS

B.B., T.B.F., M.W.K. and Y.N. designed the study. R.J.M., T.B.F and A.U.R. analyzed data from human subjects. M.C.K. performed single-cell experiments; E.T.B., R.J.M., and B.B. performed the RNA-seq analyses; Y.N. performed all other experiments. All authors contributed to writing of the manuscript.

DECLARATION OF INTERESTS

The authors declare no competing interests.

DATA AND SOFTWARE AVAILABILITY

RNA-seq data are available in the Gene Expression Omnibus repository under SuperSeries number GSE111606.

exon into the *Rest* mRNA is essential for the derepression of many neuronal genes. Heterozygous deletion of this alternative exon of mouse *Rest* causes hair cell degeneration and deafness, and the HDAC inhibitor SAHA (Vorinostat) rescues the hearing of these mice. In humans, inhibition of the frameshifting splicing event by a novel *REST* variant is associated with dominantly inherited deafness. Our data reveal the necessity for alternative splicing-dependent regulation of REST in hair cells, and they identify a potential treatment for a group of hereditary deafness cases.

INTRODUCTION

Repressor Element-1 (RE1) motifs are 21- to 30-bp DNA sequences located predominantly in neuronal genes, and they serve as binding sites for the RE1-silencing transcription factor (REST), also known as neuron-restrictive silencing factor (NRSF) (Chong et al., 1995; Schoenherr and Anderson, 1995). In non-neuronal cells, REST and its corepressors, coREST, histone deacetylase (HDAC)1, HDAC2, lysine-specific demethylase (LSD)1, and G9a methyltransferase (McGann et al., 2014), are vital to the repression of RE1-containing genes. In mice, ubiquitous deletion of both *Rest* alleles ($Rest^{-/-}$) causes upregulation of neuronal transcripts in non-neural tissues and embryonic lethality (Chen et al., 1998), and conditional deletion of both *Rest* alleles in the common progenitors of glia and neurons causes genomic instability and premature expression of neuronal transcripts (Nechiporuk et al., 2016). Thus, REST plays two key roles in non-neuronal cells: repressing neuronal genes and protecting genomic stability.

REST protein expression is reduced dramatically in differentiating neurons. Given that no gain-of-function mutation in *REST* has been identified in any species, *in vivo* assessments of the importance of such reductions have been based on the delivery of constitutively transcribed *REST* constructs into the CNS of mouse and chick embryos. In these studies, electroporation of CNS neurons with REST-encoding expression plasmids led to errors in commissural axon guidance in the spinal cord and stalled radial migration in the neocortex (Paquette et al., 2000; Mandel et al., 2011).

Transcriptional repression is the main mechanism whereby REST is downregulated in differentiating neurons (Ballas et al., 2005); however, REST is also inactivated through alternative splicing of its pre-mRNA in both neurons and mechanosensory hair cells of the ear (Raj et al., 2011; Nakano et al., 2012). The contribution of this splicing event to the reduction of REST activity was not determined in any tissue prior to this study, and its impact on organ function has not been evaluated.

Alternative splicing produces forms of the *REST* mRNA that either contain or lack exon 4. Incorporation of this exon into the *REST* mRNA requires SRRM4, a splicing regulator expressed selectively in neurons and hair cells (Calarco et al., 2009; Nakano et al., 2012). Notably, the position of the splice acceptor site of exon 4 is not identical in all mammals, and thus the length of this exon is not uniform across species. In mice exon 4 is a 16-nt frameshift-causing exon (Raj et al., 2011) (Figure 1A), whereas in humans two alternative splice donor sites exist and two forms of the exon are produced (Palm et al., 1999). Splicing of human *REST* at a donor site that is conserved between mice and humans produces a 50-nt exon with a stop codon (exon 4a), and splicing of human *REST* at a non-conserved donor

site produces a 4-nt frameshifting microexon (exon 4b). Although all exon 4-containing *REST* transcripts encode inactive proteins that lack a repressor and three zinc-finger domains of the full-length isoform (Magin et al., 2002), exon 4 is rarely considered in analyses of the *REST* exon-intron structure, perhaps because none of the vertebrate genomes in the RefSeq database are annotated for it.

Here we set out to determine whether inactivation by alternative splicing is redundant with other mechanisms of REST regulation. We found that mice heterozygous for exon 4 deletion have no apparent CNS defects but lose all mechanosensory hair cells in the ear and fail to respond to sound. The exceptional sensitivity of the ear to exon 4 deletion correlated with the particularly high contribution of exon 4 splicing to REST downregulation in hair cells. Hair cells and hearing of exon 4-knockout mice were rescued by treatment with SAHA (Vorinostat), an FDA-approved inhibitor of HDACs. Finally, analysis of the cause of dominantly inherited deafness in humans whose hearing loss was linked to the *REST*-containing *DFNA27* locus (Peters et al., 2008) revealed a novel variant of *REST* that prevented exon 4b-dependent inactivation of the encoded protein. Our data indicate that alternative splicing is essential for REST regulation in the inner ear and that defects in this mechanism can be offset by HDAC inhibitors.

RESULTS

Rest Exon 4 Is Necessary for the Development and Maintenance of Mechanosensory Hair Cells

We used homologous recombination in embryonic stem cells (ESCs) to generate mice heterozygous for a *Rest* allele in which exon 4 is flanked by loxP sites ($Rest^{+/flEx4}$; Figures 1B, S1A, and S1B). RT-PCR analysis of the neocortex of homozygous $Rest^{flEx4/flEx4}$ and wild-type (WT) mice demonstrated that insertion of loxP sites did not affect splicing of exon 4 into the mRNA (Figures S1C and S1D). An exon 4-deleted form of *Rest* ($Rest^{\Delta Ex4}$) was created by crossing $Rest^{flEx4/flEx4}$ mice to transgenic mice expressing Cre recombinase under the control of a ubiquitously active *β-actin* promoter (Figures 1B and S1E). RT-PCR analysis of neural and non-neural tissues of $Rest^{\Delta Ex4/\Delta Ex4}$ and WT mice confirmed that this deletion prevented production of the exon 4-containing splice form ($Rest^{4}$) without reducing expression of the form lacking this exon ($Rest^{4-}$; Figures 1C and S1F).

Heterozygous $Rest^{+/\Delta Ex4}$ mice exhibited balance defects and were deaf (Figures 1D–F). Histological analysis of the inner ear of $Rest^{+/\Delta Ex4}$ mice revealed that hair cells were present until embryonic day (E)16–17 but degenerated throughout the inner ear by post-natal day (P)12 (Figures 1G, 1H, S1G, S1H, and S2). The autonomy of the hair cell defect was tested by intercrossing the $Rest^{+/flEx4}$ mice to $Gfi1^{+/Cre}$ mice, which express Cre selectively in hair cells (Yang et al., 2010). As in the case of global heterozygous deletion of exon 4, hair cell-specific deletion of one copy of exon 4 led to degeneration of hair cells (Figure S1I) and deafness (data not shown). Thus, *Rest* exon 4 is essential for hair cell development and this function is cell autonomous.

Next, we tested whether deleting one copy of *Rest* exon 4 when the ear is fully developed affects hearing. $Rest^{flEx4/flEx4}$ mice were crossed to mice homozygous for a transgene

encoding tamoxifen-inducible Cre recombinase in the *Rosa26* locus ($Rosa^{CreERT2/CreERT2}$), and the offspring were treated with tamoxifen or control vehicle from P40 to P47. One month later, measurement of auditory brainstem responses (ABRs) to various pure-tone stimuli revealed hearing loss in the tamoxifen-injected $Rest^{+/flEx4};Rosa^{+/CreERT2}$ mice, but not in vehicle-injected mice of the same genotype (Figure 1I). Histological analyses of the inner ear of tamoxifen-injected $Rest^{+/flEx4};Rosa^{+/CreERT2}$ mice revealed partial loss of hair cells (Figures 1J and S3A), and PCR testing of the organ of Corti demonstrated that tamoxifen-dependent recombination occurred in some copies of the $Rest^{flEx4}$ allele (Figure S3B), consistent with reports of mosaic Cre activation in other organs (Hameyer et al., 2007). Thus, *Rest* exon 4 is critical for hair cell survival in both newborn and adult mice.

Immunofluorescence analysis of the hearing organ of P6 $Rest^{+/\Delta Ex4}$ mice revealed expression of the active form of the pro-apoptotic executioner caspase-3 in many hair cells (Figure S3C). Activation of the apoptotic pathway was confirmed by the fact that the caspase inhibitors Z-DEVD-FMK and Z-VAD-FMK delayed the death of hair cells in organ of Corti cultures derived from $Rest^{+/\Delta Ex4}$ mice. However, these inhibitors failed to prevent the degeneration of stereocilia (Figures S3D and S3E), suggesting that the inhibition of apoptosis is insufficient to rescue hair cells of $Rest^{+/\Delta Ex4}$ mice.

Although Rest is alternatively spliced in the developing neocortex, H&E staining of brain sections from $Rest^{+/\Delta Ex4}$ mice did not reveal pathological alterations (Figure S3F). The lack of histological defects in the CNS was further supported by immunostaining of brain sections from newborn $Rest^{+/\Delta Ex4}$ mice with antibodies against markers of various cortical layers (Figure S3G–S3I), as well as by immunostaining of neural tubes of such mice with an antibody against the commissural axon marker TAG-1 (Figure S3J). Thus, *Rest* exon 4 is not essential for either radial migration in the neocortex or commissural-axon pathfinding in the spinal cord.

An Intronic C > G Variant in Human *REST* Is Associated with Progressive Hearing Loss

We previously mapped dominantly inherited postlingual progressive hearing loss in a family (LMG2) to the *REST*-containing *DFNA27* segment of chromosome 4 (Peters et al., 2008). The *DFNA27* locus encompasses seven annotated genes in addition to *REST.* Sequencing of all annotated exons in the *DFNA27* locus of affected individuals failed to identify potentially pathogenic variants (data not shown), but sequencing of conserved intronic regions of *REST* revealed a C > G variant 21 bases upstream of exon 4a/b (chromosome [chr]4:56,927,594 in GRCh38 assembly; Figure 2A). This intronic variant co-segregated with hearing loss in the LMG2 family (Figure 2B). The outcomes of three additional analyses were consistent with the notion that the C > G variant is pathogenic: the C nucleotide is conserved in all 80 genomes listed in the UCSC Genome Browser as containing a region similar to exon 4 of *REST*, the G variant is absent from the Genome Aggregation Database, and sequencing of 400 DNA samples (Coriell Human Diversity Panel) invariably detected C 21 bases upstream of exon 4a/b. Thus, a rare sequence variant in the third intron of *REST* co-segregates with hearing loss in the LMG2 family.

The C > G variant causes an AC-to-AG change downstream of a polypyrimidine tract, a sequence combination that is the hallmark of splice acceptor sites. To determine whether the

AG sequence affects *REST* splicing, we performed RT-PCR analysis of blood cell RNA for a control and 2 affected subjects. RT-PCR amplification of the exon 3–5 junction region of the *REST* mRNA produced a single product for the control subject but two for the affected subjects (Figure 3A). The longer product, which was observed only for the affected subjects, contained a mutant form of exon 4a (designated exon $4a^{M}$) with an in-frame stop codon. The splice acceptor site of exon $4a^{M}$ was at the variant AG sequence, and the splice donor site was identical to that of exon 4a (Figure 3E). The shorter product was identified as the amplicon of the WT $REST^{4-}$ mRNA (Figures 3A and 3B). Thus, the C > G variant causes truncation of the coding region of *REST* in a non-neural tissue by generating a novel splice acceptor site for exon 4a. However, heterozygosity for the exon $4a^{M}$-dependent inactivation of REST is unlikely to explain the DFNA27 phenotype, because the hearing threshold of heterozygous *Rest* knock-out ($Rest^{+/-}$) mice (Gao et al., 2011) is similar to that of WT littermates at P130 (Figure S3K). Thus, we tested the C > G *DFNA27* variant for additional defects in *REST* pre-mRNA processing in the presence of SRRM4, which regulates alternative splicing of exon 4.

The Intronic C > G Variant Prevents SRRM4-Dependent Inactivation of REST

Splicing of exon 4 into the *REST* mRNA is normally tissue specific and requires SRRM4, which is expressed selectively in neurons and hair cells. SRRM4 binds to pre-mRNAs at UGC motifs located between polypyrimidine tracts and downstream alternative exons (Nakano et al., 2012; Raj et al., 2014), and when it does so the alternative exon is incorporated into the mature mRNA. We used minigenes to test the effects of SRRM4 on alternative splicing of the C > G *DFNA27* variant of *REST*. WT and *DFNA27* versions of the minigene were created by inserting *REST* exon 4a/b and its flanking introns, from a control subject and an affected subject, respectively, between two constitutively spliced exons (Figure 3C, top). The non-neuronal cell line HEK293 was co-transfected with the minigene and either an SRRM4-encoding plasmid or an empty control expression vector. Splicing of the minigene-encoded transcript in transfected cells was analyzed by RT-PCR using primers that annealed to the constitutive exons of the minigenes. In the absence of SRRM4 expression, RNA encoded by the WT minigene contained only constitutive exons (splice form 4-) and RNA encoded by the *DFNA27* minigene contained exon $4a^{M}$. In the presence of SRRM4, two splice forms were expressed from the WT minigene: one containing exon 4a and another containing the exon 4b microexon (Figures 3C–3E). The ratio of exon 4a- and exon 4b-containing splice forms was approximately 6 to 1 in the transfected cells; a similar ratio of exon 4a- and exon 4b-containing *REST* transcripts was detected in human fetal brain (Figures S3L and S3M). In the presence of SRRM4, two RNA splice forms were also expressed from the *DFNA27* minigene: an exon $4a^{M}$-containing form (longer), and a novel form that contained a 24-nt variant of exon 4b (i.e., exon $4b^{M}$; shorter). The splice acceptor site of exon $4b^{M}$ was at the *DFNA27*-specific AG, and its splice donor site was identical to that of exon 4b (Figures 3D–3F). Thus, the splicing of exon $4b^{M}$ required both C > G variant-dependent relocation of the splice acceptor site and an SRRM4-dependent shift in the splice donor site. Exon $4b^{M}$ encodes 8 amino acids and does not alter the reading frame (Figure 3E). We hypothesized that inclusion of exon $4b^{M}$ in the *REST* mRNA leads to the production of a functional $REST^{4bM}$ protein.

To test the gene repressor activity of each REST isoform, we co-transfected Neuro2a cells (which contain little endogenous REST) with it and a reporter of REST activity. The reporter contains an RE1 sequence upstream of a luciferase expression cassette (Figure 3G). Immunoblot analysis of the transfected cells demonstrated comparable expression of the REST isoforms (Figure S3N). Measurement of luciferase activity (Figure 3G) revealed that 2 of 5 isoforms were active: the $REST^{4-}$ form, which was produced only in the absence of SRRM4; and the aberrant $REST^{4bM}$ form, which was produced only in SRRM4-expressing cells and in the presence of the C > G *DFNA27* variant. These data suggest that the C > G *DFNA27* variant has opposing effects on REST depending on whether or not SRRM4 is present. In cells that do not express SRRM4, the C > G variant inactivates REST aberrantly by creating a novel acceptor site for constitutive splicing upstream of exon 4a/b. In cells that do express SRRM4, the C > G variant aberrantly leads to the production of active REST, because no stop codon is present in the 24-base region between the C > G variant-generated splice acceptor site and SRRM4-dependent splice donor site of exon $4b^{M}$. Our results strongly suggest that SRRM4-directed alternative splicing of exon 4 cannot inactivate REST in human subjects whose genome harbors the C > G *DFNA27* variant.

The *Rest*$^{\Delta Ex4}$ Mutation Is Associated with Abnormally High REST Activity in the Ear

We used the *Rest*$^{+/\Delta Ex4}$ mouse to identify exon 4-dependent alterations in the inner ear transcriptome at E15.5, a time corresponding to the onset of hair cell degeneration in the mutant mice (Figure S2C). RNA was isolated from the utricle, because in *Rest*$^{+/\Delta Ex4}$ mice the onset of hair cell degeneration in this structure is more synchronous than in the cochlea. RNA sequencing (RNA-seq) analysis of utricular samples identified 357 genes that are differentially expressed in *Rest*$^{+/\Delta Ex4}$ and WT mice (Figure 4A; Table S1). Analysis of the same data for alternative splicing patterns of mRNAs other than *Rest* did not reveal differences between the two groups (Figure S4A). Thus, the *Rest*$^{+/\Delta Ex4}$ genotype is associated with changes in utricular gene expression.

To identify REST targets among the differentially expressed genes, we used a filtered set of REST chromatin immunoprecipitation sequencing (ChIP-seq) data from ENCODE (STAR Methods), and we located REST-binding sites in 744 genes across the genome (Table S2). We refer to the 744 genes as high-confidence REST targets. Among 357 genes differentially expressed in the utricles of WT and *Rest*$^{+/\Delta Ex4}$ mice, 64 were high-confidence REST targets (red bars in Figure 4A; Table S1). The set of high-confidence REST target genes represented 25% of all genes that are expressed at reduced levels in utricles of *Rest*$^{+/\Delta Ex4}$ mice; such genes represent only 3.6% of all genes expressed in hair cells (Scheffer et al., 2015) (Fisher's exact test, $p < 0.0001$; further analyses in Figures S4B and S4C). Thus, the expression of several high-confidence REST targets is abnormally low in the utricles of *Rest*$^{+/\Delta Ex4}$ mice at the onset of hair cell degeneration.

Searches of various genotype-phenotype databases (Table S1) revealed that disorders of hearing or balance have been linked to 31 of the genes that we found to be differentially expressed in the utricles of *Rest*$^{+/\Delta Ex4}$ and WT mice (Figure 4A). Furthermore, 20 of these are required specifically for hair cell development and function (Table S1). Thus,

incorporation of exon 4 into *Rest* is necessary for the regulation of several genes that encode proteins critical for development and function of hair cells.

Heterozygous Deletion of *Rest* Exon 4 Causes Defects in the Cilia of Utricles

Our analysis of Uniprot keyword annotations of genes expressed at reduced levels in the utricles of $Rest^{+/\Delta Ex4}$ mice revealed the lowest p values to be associated with the keywords synapse and cilium (Figure 4C). Although REST was known to regulate the expression of many synaptic proteins (Ballas et al., 2005), it had not been linked to ciliogenesis. A review of genes associated with the keyword 'cilium' showed that 12 stereocilium-related and 37 kinocilium-related genes are expressed at reduced levels in the utricles of $Rest^{+/\Delta Ex4}$ mice (Table S1). High-confidence REST targets were more frequent among the stereocilium-related (25%) versus kinocilium-related (8%) genes.

Given that RFX2–4 and RFX7 regulate the transcription of many kinocilium-related genes (Manojlovic et al., 2014), we examined the differentially expressed genes and all hair cell-expressed genes for evolutionarily conserved sequences similar to RFX-binding motifs. Such sequences were present in 23% of genes expressed at reduced levels in the utricles of $Rest^{+/\Delta Ex4}$ mice but in only 9.6% of all genes expressed in utricular hair cells (Fisher's exact test, $p < 0.0001$; Tables S1 and S3; Figures S4D and S4E). These data suggest that alternative splicing of *Rest* affects utricular expression of several RFX targets. Our RNA-seq and qRT-PCR analyses also revealed reduced expression of *Rfx7* in the utricle of $Rest^{+/\Delta Ex4}$ mice (Figure S4C). Although *Rfx7* is not a high-confidence REST target, an RE1-like sequence from this gene conferred REST-dependent repression to a reporter (Figures S4F and S4G). These data are consistent with REST modulating the expression of an RFX family transcription factor in the ear.

We next examined cilia in utricles of $Rest^{+/\Delta Ex4}$ and WT mice at E15 and E16. Stereocilia were identified by F-actin staining, and kinocilia were labeled using an antibody against acetylated α-tubulin. Confocal microscopy revealed that both organelles were abnormally short in the utricles of $Rest^{+/\Delta Ex4}$ mice at E15 and E16 (Figures 4D–4F). Thus, the abnormally low expression of many stereocilium- and kinocilium-related genes in the utricles of $Rest^{+/\Delta Ex4}$ mice is associated with the shortening of both organelles.

Contributions of Alternative Splicing and Transcriptional Repression to REST Downregulation Differ between Hair Cells and Cortical Neurons

We assessed the effect of the $Rest^{\Delta Ex4}$ mutation on gene expression in the neocortex, which we selected as a reference neural tissue. RNA-seq analysis of neocortices of E15.5 WT and $Rest^{+/\Delta Ex4}$ mice revealed differential expression of 100 genes (Figure 4B). Among these, 15 were high-confidence REST targets, and expression of 10 of the 15 was moderately (i.e., <2-fold; Table S4) reduced in the $Rest^{+/\Delta Ex4}$ neocortex. For high-confidence REST targets randomly selected from the cortical and utricular RNA-seq datasets, qRT-PCR analysis at additional time points demonstrated that expression in the $Rest^{+/\Delta Ex4}$ neocortex was reduced at E16, but not P6 and P16 (Figure S4H). In contrast, expression in the utricle and saccule was reduced even at P16 following tamoxifen-induced deletion of exon 4 at P7–P9 (Figures S4H and S4I). These data suggest that the impact of exon 4 splicing on the expression of

high-confidence REST targets differs between hair cells and cortical neurons, with respect to both magnitude and duration.

RT-PCR analysis of *Rest* exon 4 splicing showed that, whereas the $Rest^{4}$:$Rest^{4-}$ ratio declined between E16 and P16 in the neocortex, it did not decline after birth in the inner ear (Figure 5A). Given that exon 4 is not spliced into *Rest* in non-neuronal cells, the $Rest^{4}$:$Rest^{4-}$ ratio is likely affected by the relative numbers of neuronal versus non-neuronal cells in the analyzed tissue. Thus, we chose to evaluate *Rest* promoter activity on a cell-by-cell basis. We used a mouse line that harbors a *Rest promoter-EGFP* transgene (Gong et al., 2003), in which an EGFP-coding sequence is present downstream of the *Rest* start codon (Figure 5B). The activity of the transgenic *Rest* promoter was evaluated based on the intensity of EGFP immunofluorescence in sections of the neocortex and inner ear. Neurons and hair cells were identified using anti-NeuN and anti-MYO7A antibodies, respectively. In cortical sections from P0 transgenic mice, the EGFP signal varied among individual neurons, representing from 2 to 60% of the EGFP signal in non-neurons. By P16, the neuronal EGFP signal was reduced to 0.4–7% of that in non-neurons (Figures 5C and 5E). In the ear, the EGFP signal in inner hair cells (IHCs) and utricular hair cells at both P0 and P16 was still 50% that in non-hair cells (non-HCs; Figures 5D and S4J); in outer hair cells (OHCs) the signal increased between P0 and P16 (Figure 5E). These data suggest that promoter-dependent downregulation of *Rest* is much stronger in cortical neurons than hair cells.

Single-Cell qRT-PCR Identifies Alternative Splicing as a Major Mechanism of REST Inactivation in Hair Cells

Given that hair cells were not previously evaluated for *Rest* expression, we used a second approach to confirm the transgene-based assessment of *Rest* transcription in the hearing organ. Multiplex single-cell qRT-PCR (scqRT-PCR) was selected because it has the potential to reveal changes in both the expression and splicing of *Rest* in individual cells. Single cells from enzymatically dissociated organs of Corti of P1 and P7 WT mice were captured on fluidics circuits and lysed. Following reverse transcription, a specific set of cDNA targets was quantified by multiplex qPCR. The set of quantified cDNA segments included a region shared by $Rest^{4}$ and $Rest^{4-}$ (i.e., total *Rest*), the exon 4–5 junction region unique to $Rest^{4}$, and the exon junction regions of several cell-type-specific transcripts (for assignment of cell type). This analysis revealed that at P7 total *Rest* expression was comparable in non-HCs, IHCs, and OHCs, whereas at P1 it was comparable in only non-HCs, IHCs, and a subset (70%) of OHCs (Figure 5F). In the remaining 30% of P1 OHCs the *Rest* mRNA was undetectable. This analysis also revealed that 94% of *Rest*-expressing hair cells, but fewer than 1% of non-HCs, contained the $Rest^{4}$ splice form (Figure 5F). Thus, *Rest* expression was high in IHCs and upregulated in OHCs during the first post-natal week. In addition, the $Rest^{4}$ splice form was specific to hair cells in the organ of Corti.

The single cell cDNAs were analyzed further by PCR to determine what percentage of *Rest* mRNAs in cochlear cells contain exon 4. At P1, ~70% of *Rest* mRNA in IHCs were $Rest^{4}$, whereas in OHCs both the expression and splicing of *Rest* were variable (Figures 5F–5H). By P7 all OHCs expressed *Rest* and 92–100% of *Rest* mRNA in both IHCs and OHCs was

the *Rest*^{4} form, but in non-HCs *Rest*$^{4-}$ was the only detected splice form. Thus, although the *Rest* gene is transcribed in all IHCs and OHCs by the end of the first postnatal week, expression of the exon 5-encoded segment of REST, which is critical to its repressor activity, was minimal due to the incorporation of exon 4 into the transcript. Overall, our expression data reveal differences in the regulation of REST in hair cells versus cortical neurons: transcriptional silencing is the predominant form of REST downregulation in cortical neurons, and alternative splicing (inclusion of exon 4) is the main mechanism of REST inactivation in hair cells.

HDAC Inhibitors Rescue OHCs of *Rest* Exon 4-Deficient Mice in Organ Cultures

Considering that HDAC1 and HDAC2 are critical for REST-dependent gene repression (McGann et al., 2014), we examined the ability of HDAC inhibitors to modulate REST activity. We tested three inhibitors: FK228 (HDAC1–3, 10-, and 11-selective) (Ganesan, 2015), SAHA (pan-HDAC), and Merck60 (HDAC1 and HDAC2 selective) (Methot et al., 2008). In HEK293 cell cultures, all three inhibitors increased the expression of nearly all eight REST targets that were selected for qRT-PCR analysis based on reduced expression of their orthologues in the ear and brain of the *Rest*$^{+/\Delta Ex4}$ mouse (Figure S5A). Thus, the effects of FK228, SAHA, and Merck60 on the expression of REST target genes were similar to those of splicing exon 4 into *Rest*.

We used an organ culture system to test the effects of all three HDAC inhibitors on the hair cells of *Rest*$^{+/\Delta Ex4}$ mice. Organ of Corti cultures from P1 *Rest*$^{+/\Delta Ex4}$ and WT mice were incubated with 2 nM FK228, 1 μM SAHA, 1.2 μM Merck60, or solvent (non-treated group) from the second day *in vitro* (DIV2) to DIV8. F-actin staining of these cultures at DIV9 revealed that, whereas in non-treated organ cultures from *Rest*$^{+/\Delta Ex4}$ mice the stereocilia of most OHCs degenerated, in HDAC inhibitor-treated cultures from the same mouse line most OHCs retained stereocilia (Figures 6A, 6B, and S5B). Thus, HDAC inhibitors prevented the degeneration of OHCs of *Rest*$^{+/\Delta Ex4}$ mice *in vitro*.

Next, we analyzed the effects of FK228 on the transcriptomes of organ of Corti cultures. FK228 was selected for this experiment for two reasons: it inhibits fewer HDACs than SAHA, and it is available from multiple commercial resources while Merck60 is not. RNA-seq analysis of FK228-treated and non-treated organ of Corti cultures from *Rest*$^{+/\Delta Ex4}$ and WT mice revealed treatment-dependent alterations in the expression of ~8,000 genes, independent of the genotype of the mouse of origin (Table S5). Among these genes, and also among the genes that are differentially expressed in the utricles of *Rest*$^{+/\Delta Ex4}$ and WT mice, those that were high-confidence REST targets or contain potential binding sites for RFX were predominantly upregulated (Figures S5C–S5G). Thus, FK228 is capable of upregulating subsets of genes that are expressed at reduced levels in the ears of *Rest*$^{+/\Delta Ex4}$ mice.

The fact that FK228 alters the expression of many genes that are unaffected in *Rest*$^{+/\Delta Ex4}$ mice raised the possibility that the observed rescue of *Rest*$^{+/\Delta Ex4}$ OHCs could result from a block in a general cell death pathway. To test this possibility, we added FK228 to organ of Corti cultures derived from newborn *Gfi1*$^{-/-}$ mice, whose IHCs (like the OHCs of *Rest*$^{+/\Delta Ex4}$ mice) are subject to post-natal apoptotic cell death (Wallis et al., 2003). F-actin

staining of organ of Corti cultures incubated with FK228 demonstrated that this inhibitor did not rescue the IHCs of *Gfi1*$^{-/-}$ mice (Figure S6A). Thus, the ability of FK228 to rescue hair cells from degeneration depends on the specific molecular cause of the hair cell defect.

SAHA Rescues Hair Cells and Hearing in *Rest* Exon 4-Deficient Mice

HDAC inhibitors have not been examined for their abilities to cross the blood-perilymph barrier (BPB); however, a few have been studied for their ability to penetrate the BPB-like blood-brain barrier (BBB). These studies have shown that, although SAHA has a low brain-to-plasma ratio, it is more effective at crossing the BBB than other commercially available HDAC inhibitors (Hanson et al., 2013). Thus, we tested SAHA for the ability to rescue the OHCs of *Rest*$^{+/\Delta Ex4}$ mice *in vivo*, injecting mice subcutaneously with SAHA or vehicle (solvent) at P2, P4, and P5. F-actin staining of the organ of Corti of vehicle-injected *Rest*$^{+/\Delta Ex4}$ mice revealed that most OHCs lacked stereocilia at P6. In contrast, in the SAHA-injected *Rest*$^{+/\Delta Ex4}$ mice, most OHCs retained these structures (Figures 6C, 6D, and S6B). Thus, the OHCs of *Rest*$^{+/\Delta Ex4}$ mice can be rescued *in vivo* by systemically administered SAHA.

Given that in *Rest*$^{+/\Delta Ex4}$ mice the IHCs had degenerated by the time of SAHA injection, we tested IHC survival in organs of Corti that were exposed to HDAC inhibitors from the time of deletion of *Rest* exon 4. Organ of Corti cultures from P5 WT and *Rest*$^{+/flEx4}$;*Rosa*$^{+/CreERT2}$ mice were incubated with tamoxifen or solvent at DIV3 and DIV4 (Figure 6E). A subset of these cultures was also incubated with FK228 or SAHA from DIV3 to DIV11. F-actin staining of these cultures at DIV12 demonstrated that SAHA and FK228 prevented the tamoxifen-dependent degeneration of IHCs and OHCs of *Rest*$^{+/flEx4}$;*Rosa*$^{+/CreERT2}$ mice (Figures 6E and S6D). PCR analysis of the same cultures confirmed that tamoxifen induced recombination of loxP sites in nearly all copies of the *Rest*$^{+/flEx4}$ allele, independent of whether an HDAC inhibitor was present (Figure S6C). Thus, both IHCs and OHCs in *Rest* exon 4-deficient organ of Corti cultures can be rescued by exposure to HDAC inhibitors.

We assessed the effects of SAHA on the hearing of mice in which exon 4 was deleted post-natally. *Rest*$^{+/flEx4}$;*Rosa*$^{+/CreERT2}$ and WT mice were injected subcutaneously with tamoxifen or vehicle from P7 to P9 and also with SAHA or vehicle daily from P7 to P15 (Figure 6F). At P16, hearing was tested using pure-tone stimuli and ABR recordings. The ABR analysis revealed that SAHA reduced the tamoxifen-dependent shift in hearing threshold of *Rest*$^{+/flEx4}$;*Rosa*$^{+/CreERT2}$ mice at low sound frequencies (Figure 6G). Histological analysis of cochleas of the same mice demonstrated that SAHA reduced the extent of tamoxifen-dependent hair cell loss (Figures 6F and S6E). In WT mice, tamoxifen affected neither hearing nor the survival of hair cells. Thus, SAHA alleviated the cochlear defects associated with the deletion of *Rest* exon 4.

Given that SAHA was more effective in rescuing the OHCs of *Rest* exon 4-deficient mice at P6 than P16 (Figures 6D and 6F), we tested the effects of SAHA injection on acetylation of histone H4 in OHCs at P6 and P16. Immunofluorescence analysis showed that SAHA injection led to an increase in H4 acetylation at both time points; however, at P6 the magnitude of the increase was ~6-fold larger than at P16 (Figure S6F). In rodents the BPB

develops between P4 and P14 (Suzuki et al., 1998), and thus hair cells may be more accessible to systemically delivered SAHA at P6 than P16.

DISCUSSION

Here we identify *REST* as a novel deafness gene in humans, and we show that the deafness-causing variant prevents inactivation of the REST protein by alternative splicing. We also show that a mouse model of the *REST* splicing defect is characterized by deafness and degeneration of mechanosensory hair cells, and we demonstrate that both hair cells and hearing can be partially rescued in these mice by applying the HDAC inhibitor SAHA. Overall, our data indicate that alternative splicing is critical for REST inactivation in hair cells and that defects in this mechanism can be offset by chemical inhibition of HDACs.

Although mutations in the constitutively spliced exons of *REST* have been linked to cancer and gingival fibromatosis (Mahamdallie et al., 2015; Bayram et al., 2017), ours is the first study to associate REST with hearing loss, and *DFNA27* is the first genetic variant shown to affect the alternative splicing of REST. The effects of the *DFNA27* variant are highly unusual in that either gain or loss of function of the encoded protein occurs depending on the cellular context. In cells expressing the splicing factor SRRM4, the variant prevents REST inactivation by alternative splicing (gain of function), whereas in cells lacking SRRM4 it causes REST inactivation (loss of function). Our study suggests that the gain-of-function effect of *DFNA27* is deafness causing because selective prevention of alternative splicing-dependent inactivation of mouse REST also leads to deafness (Figure 1). In addition, in mice heterozygous for deletion of the first coding exon of *Rest* (*Rest*$^{+/-}$) the hearing threshold is similar to those of WT littermates, at least until P130 (Figure S3K). Thus, heterozygosity for loss-of-function mutations in *REST* may not impair hearing in humans.

Our results provide a plausible explanation for an apparent discrepancy: *DFNA27*-associated hearing loss is postlingual and progressive, yet *Rest*$^{+/\Delta Ex4}$ mice are deaf by the time of normal hearing onset (i.e., P12–P16). Specifically, our results indicate that, whereas the mouse *Rest*$^{\Delta Ex4}$ mutation completely prevents exon 4-dependent inactivation of the encoded protein, the human *DFNA27* variant prevents exon 4b-dependent inactivation of REST without inhibiting exon 4a-dependent truncation of the encoded protein.

Our data shed new light on *Srrm4* regulation in the ear. Although *Srrm4* is repressed by REST in several cell types (Raj et al., 2011), in the hair cells of *Rest*$^{+/\Delta Ex4}$ mice increased REST activity is not associated with reduced *Srrm4* expression. Given that the *Srrm4* promoter contains binding sites for the transcription factor ATOH1 and its binding dramatically induces *Srrm4* expression in hair cells (Cai et al., 2015), we speculate that in developing hair cells ATOH1 predominates over REST in regulating *Srrm4*.

Our findings also have implications for the cause of the inner ear defects in the Bronx waltzer (bv) mouse line. In this line, an *Srrm4*-truncating mutation (*Srrm4*$^{bv/bv}$) is associated with degeneration of most hair cells, as well as impaired hearing and balance (Nakano et al., 2012). In the balance organs of *Srrm4*$^{bv/bv}$ mice, the incorporation of *Rest* exon 4, as well as that of alternative exons of ~50 other genes, is abnormally inefficient. Based on our current

analysis, we speculate that the reduced incorporation of *Rest* exon 4 is one of multiple causes of the degeneration of hair cells in *Srrm4*$^{bv/bv}$ mice.

RNA-seq analysis of utricles of *Rest*$^{+/\Delta Ex4}$ mice revealed reduced expression of over 20 genes that are required for hearing and/or balance. Given that none of the previously characterized mutations in these genes is associated with hair cell loss of the same severity as the *Rest*$^{\Delta Ex4}$ mutation, the hair cell degeneration observed in *Rest*$^{+/\Delta Ex4}$ mice is unlikely to be caused by reduced expression of a single characterized gene. Thus, we speculate that reduced expression of multiple genes contributes to the hair cell defect in *Rest*$^{+/\Delta Ex4}$ mice. Our RNA-seq data also indicate that alternative splicing of *Rest* affects both the neuronal and non-neuronal sectors of the hair cell transcriptome. Nearly half of the genes expressed at reduced levels in the *Rest*$^{+/\Delta Ex4}$ utricle are either high-confidence REST targets or potential RFX targets. Whereas most of high-confidence REST targets are transcribed selectively in neurons and hair cells, many of the potential RFX target genes encode kinocilium-related proteins that are not expressed in neurons. Given that nearly all of these kinocilium-related genes lack high-confidence binding sites for REST and are co-expressed with *Rest* in multi-ciliated epithelia, we suggest that the effect of REST on these genes in hair cells is indirect and cell type specific.

DFNA27 is the first example of a non-syndromic, deafness-causing gene defect whose consequences can be ameliorated in a model organism by applying SAHA, an FDA-approved compound for the treatment of cutaneous T cell lymphomas (Mann et al., 2007); however, many other HDAC inhibitors have been developed. Some of those that were developed most recently and are not yet commercialized have better tissue penetration and HDAC1 and HDAC2 selectivity than SAHA (Wagner et al., 2015). We suggest that these compounds hold promise for providing therapeutic benefits in cases of progressive hearing loss caused by gain-of-function mutations in *REST*.

STAR Methods

CONTACT FOR REAGENTS AND RESOURCE SHARING

Further information and requests for resources and reagents should be directed to and will be fulfilled by the Lead Contact, Botond Bánfi (botond-banfi@uiowa.edu).

EXPERIMENTAL MODEL AND SUBJECT DETAILS

Human Subjects—All human subjects-related procedures were approved by the Combined Neuroscience Institutional Review Board at the National Institutes of Health (NIH), Bethesda, MD, USA. Written informed consent was obtained from all participants. Venous blood was collected from the study subjects for DNA and RNA isolations. The ages of subjects were between 14 and 72 at the time of blood collection. The number and gender of participating subjects are shown in Figure 2B. Audiometric data for the participating subjects were described previously (Peters et al., 2008).

Mice—All mouse procedures were approved by the University of Iowa Institutional Animal Care and Use Committee. Mice were housed in groups in temperature controlled rooms (21 ± 2°C) with 12 h/12 h light/dark cycle. Food and water were available for the mice *ad*

libitum. Animal husbandry and health status monitoring were provided by the Office of Animal Resources staff at the University of Iowa. The ages of tested mice are indicated in the figure legends. The sexes of pre-weaning mice were not determined. The sexes of weaned mice (P21 and older) were documented. Male and female $Rest^{+/\Delta Ex4}$ mice exhibited equally severe hearing loss and balance defect. The *Rest promoter-EGFP* transgenic mouse line was generated in the GENSAT project and made available through the Mutant Mouse Resource and Research Center (Gong et al., 2003). Heterozygous $Gfi1^{+/Cre}$ and homozygous $Gfi1^{Cre/Cre}$ mice were described previously (Yang et al., 2010). In the current study, $Gfi1^{+/Cre}$ mice were used to express Cre selectively in hair cells within the inner ear. $Gfi1^{Cre/Cre}$ mice were used for experiments shown in Figure S6A. In the $Gfi1^{Cre}$ allele, the Cre-encoding sequence replaces the protein-coding region of *Gfi1*. We refer to the $Gfi1^{Cre/Cre}$ mice as $Gfi1^{-/-}$ to emphasize that the goal was the inactivation of both *Gfi1* alleles in Figure S6A as opposed to the expression of the Cre recombinase. $Rest^{+/-}$ mice were generated by intercrossing the previously descried *Rest* exon 2-floxed mouse line with the *β-actin-Cre* transgenic mouse line (Lewandoski et al., 1997; Gao et al., 2011).

Generation of $Rest^{+/\Delta Ex4}$ Mice—Conventional gene targeting was used to insert loxP site upstream and downstream of exon 4 of *Rest* ($Rest^{flNeoEx4}$) in mouse ES cells (Figure S1A). Two recombination-positive ES cell clones were selected for the production of $Rest^{+/flNeoEx4}$ mice. Recombination of the targeting vector with the mouse genome was confirmed by PCR (see primers in Table S6) and Southern blotting, in both ES cells and $Rest^{+/flNeoEx4}$ mice. For Southern blot analysis, genomic DNA was digested with the EcoRI, SpeI or BglII restriction endonuclease (New England Biolabs). Electrophoretically separated digestion products were transferred to positively charged nylon membranes (Roche) and hybridized with digoxigenin-labeled probes. Three probes were designed: one from the neomycin-resistance gene (*Neo*) of the targeting construct, and two from genomic regions that flank the targeted segment of *Rest* (Figure S1A). Digoxigenin-labeled nucleotides were incorporated into the probes using the DIG DNA Labeling and Detection Kit (Roche). The same kit was also used for the visualization of hybridized probes, following the manufacturer's instructions. To remove *Neo* from the $Rest^{flNeoEx4}$ allele, $Rest^{+/flNeoEx4}$ mice were bred with $Rosa^{FLP1/FLP1}$ knock-in mice (Farley et al., 2000). Finally, the floxed exon was removed by intercrossing the $Rest^{+/flEx4}$ mouse line with Cre-expressing mouse lines, including *β-actin-Cre* transgenic, $Gfi1^{+/Cre}$ knock-in, and $Rosa^{+/CreERT2}$ knock-in mice (Lewandoski et al., 1997; Hameyer et al., 2007; Yang et al., 2010). In $Rest^{+/flEx4};Rosa^{+/CreERT2}$ mice, Cre recombinase activity was induced using one of two regimens of injections with (Z)-4-hydroxytamoxifen (Tocris Bioscience), depending on the age of the mice: P7–P9 mice were subcutaneously injected with (Z)-4-hydroxytamoxifen (33 mg/kg body weight) daily for 3 days; P40–P47 mice were intraperitoneally injected with (Z)-4-hydroxytamoxifen (33 mg/kg body weight) daily for 8 days.

Cell Lines and Tissue Culture—HEK293 cells (female) and Neuro2a cells (male) were obtained from the American Type Culture Collection (ATCC). HEK293 cells were grown in Dulbecco's Modified Eagle Medium/Nutrient Mixture F-12 (DMEM/F-12 from Corning). Neuro2a cells were grown in DMEM (Corning). Both DMEM/F-12 and DMEM were supplemented with 10% fetal bovine serum (FBS from Atlanta Biologicals), penicillin (100

units/mL; Thermo Fisher Scientific), and streptomycin (100 μg/mL; Thermo Fisher Scientific). Organs of Corti were dissected from P0–P5 mice and placed on Matrigel-coated transwell plates (Corning). The sexes of these mice were not determined. Organ cultures were maintained in neurobasal-A medium supplemented with B-27, N-2, 0.5 mM L-glutamine (all from Thermo Fisher Scientific), and 100 U/mL penicillin (Sigma). The culture medium was replaced on the organs once in every 3 days. Organ cultures and cell lines were grown at 37 °C in the presence of 5% CO_2.

METHOD DETAILS

Hearing and Balance Tests—The ABR thresholds of mice were measured using a previously described open-field system, and both broadband and pure-tone stimuli (Nakano et al., 2012). The ability of mice to balance (P21–P28) was evaluated by measuring the time each mouse could remain on a fixed horizontal rod (1.8 cm in diameter) following two training trials.

Isolation and Analyses of DNA and RNA—Genomic DNA was extracted from human blood samples as described previously (Peters et al., 2008). To analyze the *DFNA27* interval in the genomic DNA, two sets of PCR primers were designed. The first set was designed to amplify all annotated exons in *DFNA27* and all conserved intronic segments in *REST*. The second set was designed specifically for the amplification of the exon 4-containing region of *REST* (see primers in Table S6). The PCR amplicons were Sanger sequenced using BigDye Terminator chemistry and an ABI3730 DNA Analyzer (Applied Biosystems). RNA was isolated from human blood samples using the PAXgene Blood RNA Kit (Qiagen), and was reverse transcribed using SuperScript III reverse transcriptase (Thermo Fisher Scientific). The cDNA products were analyzed for the presence of *REST* splice variants by PCR (see primers in Table S6). The PCR products were separated by size and sub-cloned into the pCR-TOPO vector (Thermo Fisher Scientific). A total of 180 clones were sequenced using the Sanger method. For the isolation of cortical RNA from mice, the neocortex was dissected from the brain and homogenized in Trizol Reagent (Thermo Fisher Scientific). RNA was extracted from the homogenized tissue with chloroform, and precipitated with isopropanol. RNA was dissolved in water, incubated with DNAse, and further purified on the separation column of the RNeasy Mini Kit (Qiagen), following the manufacturer's instructions. RNA was isolated from vestibular maculas and HEK293 cells using either the RNeasy Micro or Mini Kit (Qiagen), depending on the number of cells in the samples. RNA samples from mice and HEK293 cells were reverse transcribed using SuperScript IV reverse transcriptase (Thermo Fisher Scientific). Human spleen RNA and fetal brain RNA were purchased from Clontech Laboratories, and were reverse transcribed using either SuperScript IV or ThermoScript (Thermo Fisher Scientific). The ratio of the detected splice forms of *REST* was not affected by the choice of reverse transcriptase (data not shown). The cDNA samples produced were analyzed by PCR and qPCR (see primers in Table S6). PCR products less than 200 bp in length were separated in polyacrylamide gels; larger PCR products were separated in agarose gels.

Immunofluorescence and Histochemistry—The following antibodies were used for the immunofluorescence assays in this study: mouse anti-acetylated tubulin (Sigma, T7451),

rabbit anti-MYO7A (Proteus Biosciences, Inc., 25-6790), mouse anti-MYO7A (University of Iowa Developmental Studies Hybridoma Bank, Myo7A 138-1), rabbit anti-H4ac (Active Motif, 39244), rabbit anti-GFP (Novus, NB600-308), mouse anti-SATB2 (Santa Cruz, sc-81376), rabbit anti-TBR1 (Abcam, ab31940), mouse anti-NeuN (Millipore, MAB377), rabbit anti-PAX6 (Biolegend, 901301), goat anti-TAG1 (R&D Systems, AF4439), rabbit anti-cleaved CASP3 (Cell Signaling, 9579), donkey Alexa 488-conjugated anti-goat (Thermo Fisher Scientific, A-11055), donkey Alexa 488-conjugated anti-mouse (Thermo Fisher Scientific, A-21202), donkey Alexa 594-conjugated anti-rabbit (Thermo Fisher Scientific, A-21207), donkey Alexa 568-conjugated anti-mouse (Thermo Fisher Scientific, A-10037), donkey Alexa 488-conjugated anti-rabbit (Thermo Fisher Scientific, A-21207). Whole-mount preparations of cochlear and vestibular tissues were fixed with 4% paraformaldehyde in PBS (4% PFA), and labeled with an anti-MYO7A antibody, an anti-H4ac antibody, an anti-acetylated-α-tubulin antibody, an anti-cleaved CASP3 antibody, or phalloidin-Alexa 488. The binding of primary antibodies to the specimens was tested using Alexa 488-conjugated, Alexa 568-conjugated, or Alexa 594-conjugated secondary antibodies. *Rest* promoter activity was examined in cortical and inner ear tissues using *Rest promoter-EGFP* transgenic mice. These mice were transcardially perfused with 4% PFA while under deep anesthesia. Inner ears and brains were dissected from the perfused mice, cryoprotected in sucrose solutions, embedded into Tissue Freezing Medium (Electron Microscopy Sciences), and cryosectioned. Sections were incubated with Alexa 488-conjugated anti-GFP antibody in combination with an Alexa 568-conjugated anti-MYO7A antibody or an Alexa 568-conjugated anti-NeuN antibody. The specificity of GFP detection was confirmed by probing inner ear and brain sections of WT mice with the Alexa 488-conjugated anti-GFP antibody. The APEX Antibody Labeling Kit (Thermo Fisher Scientific) was used for the conjugation of Alexa dyes to the antibodies. Layering of the neocortex was examined in P0 mice. Brain samples were fixed with 4% PFA, cryoprotected in sucrose solution, and embedded into Tissue Freezing Medium (Electron Microscopy Sciences). Cryosections were co-labeled with a mouse anti-SATB2 antibody and a rabbit anti-TBR1 antibody, or a mouse anti-NeuN antibody and a rabbit anti-PAX6 antibody. The binding of primary antibody was visualized with Alexa 488- and Alexa 594-conjugated secondary antibodies. For the labeling of commissural axons, mouse embryos (E11.5) were fixed with Prefer (Anatech) and processed for cryosectioning as described for the brain samples. Transverse sections of the rostral region of the spinal cord were probed with an anti-TAG1 antibody and an Alexa 488-conjugated secondary antibody. Images of fluorescently labeled tissues were acquired using an LSM 880 confocal microscope (Carl Zeiss) and analyzed using the ZEN lite 2012 software (Carl Zeiss) or ImageJ. For histochemical analysis of the brain, mice were transcardially perfused with 4% PFA while under deep anesthesia, after which the brain was dissected from the skull, embedded into paraffin, sectioned, and stained with H&E.

Single Cell RT-PCR—Cochleas were dissected from either CD-1 or *Gfi1*$^{+/Cre}$*;Rosa*$^{+/CAG\text{-}tdTomato}$ knock-in mice at P1 and P7 (the sexes of these mice were not determined). The organ of Corti-containing regions were dissected from the cochlea in ice-cold DMEM/F-12, and epithelia were removed from underlying mesenchyme following a 10-min treatment with 0.2 mg/mL thermolysin (Sigma) and 1.67 μg/mL DNase I (Stem Cell

Technologies) at 37°C. Cochlear epithelial sheets containing hair cells, supporting cells, and some surrounding non-sensory cells were dissociated by 15 min digestion with TrypLE Select (Gibco) or papain (Worthington) at 37°C and by trituration at 5-min intervals during the digestion. Enzymatic digestions were quenched with an equal volume of ice-cold DMEM/F-12 containing 10% FBS, and nuclei were stained with 1 μg/mL Hoechst 33342 (Thermo Fisher Scientific). Dissociated cells were pelleted and resuspended in the volume of DMEM/F-12 necessary to achieve a cell concentration of ~500 cells/μL. cDNA was prepared from individual cells, and specific targets were pre-amplified using the Fluidigm C1 platform and either small (5–10 μm) or medium-sized (10–17 μm) integrated fluidic chips (Fluidigm), following the manufacturer's instructions. All capture sites of the integrated fluidic chips were imaged prior to cell lysis to identify the wells that contained viable single cells. Initial captures with non-transgenic mice were stained with 4 μM Calcein AM dye (Thermo Fisher Scientific), to confirm cell viability based on esterase activity in the cytoplasm. Primers for pre-amplification and qPCR were designed with the NCBI Primer-BLAST tool or adopted from a previous study (Burns et al., 2015). Primer combinations were checked for multiplex primer dimerization using the Multiple Primer Analyzer Tool (Thermo Fisher Scientific). Single-cell cDNA samples were analyzed by qPCR on the Fluidigm BioMark HD platform (see primers in Table S6). The limit of detection (LOD) was set to Ct value 24, and expression data are reported as Log2 expression (Log2Ex) = LOD – Ct. qPCR assays were validated using a mouse universal cDNA library and a P1 mouse cochlear cDNA library, as described previously (Burns et al., 2015). Assay efficiencies were calculated as $10^{(-1/\text{slope})} - 1$ using a three-fold dilution series of pre-amplified cDNA. All assays used in this study had efficiencies between 0.926 and 1.124. Based on the expression data, cell IDs were grouped using unsupervised hierarchical clustering function of the SINGuLAR Analysis Toolset (Fluidigm) in R 3.0.2. The hair-cell representing cluster was identified based on the high average Log2Ex of 10 hair cell-specific transcripts (*i.e.*, *Chgb*, *Gfi1*, *Myo15*, *Pvalb*, *Scg3*, *Scn3b*, *Snap25*, *Srrm3*, *Srrm4*, and *Myo7a*) across the cells (Scheffer et al., 2015). The 'non-hair cell' representing cluster was identified based on the low average expression of the 10 genes. In the hair-cell cluster, IHCs were identified based on the expression of *Fgf8* (Log2Ex > 6) and the lack of expression of *Slc26a5* (Log2Ex = 0). OHCs were identified based on the expression of *Slc26a5* (Log2Ex > 4 at P1 and Log2Ex > 10 at P7) and the lack of expression of *Fgf8* (Log2Ex = 0). Cells in which both *Fgf8* and *Slc26a5* were detected were excluded from analysis.

Cloning Procedures—The *Rest* exon 4-targeting construct was assembled in the pBlueScript vector. The left arm, floxed region, and right arm of the targeting construct was amplified by PCR using the mouse BAC clone RP23–27L14 (Children's Hospital Oakland Research Institute) as template. Restriction sites were incorporated into the amplified DNA segments via PCR primers (Table S6). The *Neo* cassette was obtained from GeneBridges. The completed targeting construct was excised from pBlueScript by restriction digestion, and ES cells were electroporated with it. *REST* minigenes were generated by subcloning PCR-amplified exon 4 and its flanking introns (~350 bp in both directions), from a control subject and a DFNA27 subject, between two constitutively spliced exons in the pET-01 vector (Mobitec). For production of the REST reporter gene, the canonical RE1 motif was fused to the proximal end of the thymidine kinase promoter (TK) from the pGL4.54 plasmid

(Promega), using overlap extension PCR. The RE1-like sequence from the mouse *Rfx7* gene (*Rfx7*-RE1L, chr9:72,606,074–72,606,107; GRCm38/mm10 assembly) was inserted distal of the TK promoter in a synthetic gene block DNA (Integrated DNA Technologies, Inc.). The RE1-TK and TK-*Rfx7*-RE1L DNA fragments were subcloned into the multiple cloning site of the promoterless firefly luciferase-encoding vector pGL4.10 (Promega) to generate the RE1-TK-pGL4.10 and TK-*Rfx7*-RE1L-pGL4.10 plasmids. The negative-control reporter gene TK-pGL4.10 was generated by subcloning the TK promoter (without an RE1) into the pGL4.10 vector. Mutant version of the TK-*Rfx7*-RE1L-pGL4.10 reporter was generated by changing the 'TCC' and 'GGT' triplets of the RE1L motif to 'TTT' in a synthetic gene block and subcloning it into pGL4.10. Human SRRM4 and various isoforms of human REST were amplified by RT-PCR (see primers in Table S6) and subcloned into the pcDNA3.1+ or pLPC (Westbrook et al., 2008) expression vector.

Splicing Assays in Transfected Cells—HEK293 cells were co-transfected with the REST minigene (WT or *DFNA27* version) and an SRRM4-encoding plasmid using Lipofectamine LTX and PLUS reagent (Thermo Fisher Scientific). In some experiments, the SRRM4-encoding plasmid was replaced with an empty pcDNA3.1+ expression vector (negative control). RNA was isolated from the cells 24 h after transfection using RNeasy Mini Kit (Qiagen). The splicing of minigene-encoded transcripts was tested by RT-PCR (see primers in Table S6).

qRT-PCR Analysis of HDAC Inhibitor-Incubated Cells—HEK293 cells were incubated with SAHA (1 and 5 μM), FK228 (2 and 10 nM), Merck60 (0.6 and 1.2 μM), or DMSO (0.1%, negative control) for 36 h. During incubation with HDAC inhibitors and 0.1% DMSO, the FBS concentration in the culture medium was changed from 10% to 2% to reduce the potential binding of HDAC inhibitors to serum proteins. At the end of the 36-h incubation time, RNA was isolated using RNeasy Mini Kit (Qiagen). The expression levels of selected REST target genes and the reference gene *G6PD* were analyzed using qRT-PCR (see primers in Table S6).

Reporter Gene-Based Assays and Immunoblotting—Neuro2a cells were transfected with the luciferase-encoding plasmids RE1-TK-pGL4.10 (firefly luciferase) and pGL4.7Rluc (renilla luciferase, 10:1 ratio of the two constructs), and expression vectors encoding the WT or DFNA27 forms of REST. Both flag-tagged and non-tagged forms of the various REST forms were tested. The presence of N-terminal flag tag did not affect the results of the assay (data not shown). In another set of experiments, Neuro2a cells were transfected with TK-*Rfx7*-RE1L-pGL4.10 and pGL4.7Rluc (10:1 ratio) or TK-*Rfx7*-RE1L^{MUT}-pGL4.10 and pGL4.7Rluc (10:1 ratio), and an expression vector encoding WT REST^{4-}. Cells were lysed 36 h after transfection. The activities of firefly and renilla luciferases in the lysates were measured using the Dual-Luciferase Reporter Assay (Promega) and a luminometer (Wallac 1420 Multi-label Counter, PerkinElmer Life Sciences). Expression levels of WT and DFNA27 isoforms of REST were tested in transfected Neuro2a cells using immunoblotting. Cells were lysed in SDS sample buffer, boiled for 3 min, resolved by SDS-PAGE, and electroblotted onto nitrocellulose membranes. Following a blocking incubation step, monoclonal anti-flag antibody (Sigma, F3165, diluted

1:1,000) or rabbit anti-LMNB1 antibody (Abcam, ab16048, diluted 1:5,000) was added to the membranes for 14 hours. After multiple washing steps, membranes were incubated with HRP-conjugated anti-mouse antibody (Bio-Rad, 170-6516, diluted 1:10,000) or HRP-conjugated anti-rabbit antibody (GE Healthcare Life Science, NA934-1ML, diluted 1:10,000). Immunoblot signals were visualized using SuperSignal West Pico Chemiluminescent Substrate (Thermo Fisher Scientific).

Incubation of Organ of Corti Cultures with HDAC Inhibitors—To analyze the effects of HDAC inhibitors on the survival of cochlear hair cell *in vitro*, organ of Corti cultures were incubated with SAHA (1 μM), FK228 (2 nM), Merck60 (1.2 μM), or DMSO (0.1%) from DIV2–3 to DIV9–12. SAHA was added to the cultures every 12 h because its half-life in serum is only 1–2 h (Konsoula and Jung, 2008). FK228 was added to the organ cultures once in every 3 days for 12 h; the medium was exchanged at the end of the 12-h incubation to prevent cytotoxicity associated with the prolonged presence of FK228. The Merck60-containing medium was exchanged daily because the half-life of Merck60 in aqueous solutions has not been reported. Some of the organ cultures were also treated with 5 μM (Z)-4-hydroxytamoxifen (Tocris Bioscience) on DIV3–4 to induce Cre activity. On DIV9 or DIV12, the organ cultures were fixed with 4% PFA and labeled with phalloidin-Alexa 488 or immunostained as described in the ‘Immunofluorescence and Histochemistry’ section. To test the efficiency of tamoxifen-induced recombination of loxP sites *in vitro*, DNA was isolated from a subset of cultures at DIV12 using PicoPure DNA Extraction Kit (Thermo Fisher Scientific). The isolated DNA was analyzed using PCR (see primers in Table S6). To analyze FK228-dependent gene expression changes, organs of Corti were dissected from newborn mice and incubated with 2 nM FK228 or solvent only (0.1% DMSO) from DIV1 to DIV1.5 and from DIV3 to DIV3.5. RNA was isolated from these cultures at DIV3.5.

RNA Sequencing and Bioinformatics Analyses—The neocortex of 3 WT and 3 *Rest*$^{+/\Delta Ex4}$ mice (E15.5) was dissected from the brain, and RNA was isolated from the dissected tissue using Trizol Reagent (Thermo Fisher Scientific). RNA was further purified on the separation column of the RNeasy Mini Kit (Qiagen), following the manufacturer’s instructions. Utricles were dissected from E15.5 WT and *Rest*$^{+/\Delta Ex4}$ mice, and RNA was isolated from the dissected tissue using the RNeasy Micro Kit (Qiagen). RNA was pooled from 7–9 mice to obtain a single sample with sufficiently high concentration for RNA-seq. In total, 25 WT mice (n = 3 samples) and 32 *Rest*$^{+/\Delta Ex4}$ mice (n = 4 samples) were used for the RNA-seq experiment. The RNeasy Micro Kit (Qiagen) was used for the isolation of RNA from organ of Corti cultures that were incubated with 2 nM FK228 or solvent. RNA was pooled from 6–8 organ of Corti cultures to obtain a single sample for RNA-seq. In total, 28 WT mice (n = 4 FK228-treated and 4 control samples) and 29 *Rest*$^{+/\Delta Ex4}$ mice (n = 4 FK228-treated and 4 control samples) were used for the RNA-seq experiment. All RNA samples were processes for RNA-seq following identical protocol. 200–300 ng of total RNA were reverse transcribed using SuperScript IV reverse transcriptase (Thermo Fisher Scientific), oligo dT primer, and template switching oligo. Second strand cDNA was amplified using LongAmp DNA polymerase (New England BioLabs) for 12 PCR cycles, purified on SPRI Select Beads (Beckman Coulter), and eluted with Buffer EB (Qiagen). The

size distribution and concentration of second strand cDNA was evaluated using High Sensitivity Large Fragment Analysis Kit and a Fragment Analyzer instrument (both from Advanced Analytical). 125 pg of second strand cDNA was tagmented, PCR amplified, and indexed using the Nextera XT Library Prep Kit (Illumina). Following AMPure XP bead purification (Beckman Coulter), the size distribution and concentration of cDNA Libraries were evaluated using High Sensitivity NGS Fragment Analysis Kit (Advanced Analytical) and Fragment Analyzer. All libraries were normalized, pooled and sequenced in a HiSeq1500 instrument (126 × 126 paired end mode; Illumina). Demultiplexed samples were mapped to the mouse genome (GRCm38.p4 Release M11 from GENCODE), and transcripts were quantified using the STAR aligner (v2.5.2a) and the '–quantMode GeneCounts' parameter (Dobin et al., 2013). Gene level counts were filtered to remove genes that had lower than 5 counts in all compared samples. Differential gene expression was evaluated using the DESeq2 tool (Love et al., 2014). Genes were considered differentially expressed if the adjusted p in the DESeq2 analysis was lower than 0.05. Only the RefSeq curated genes were analyzed, and pseudogenes were filtered out. The UCSC Table Browser (Karolchik et al., 2004) was used for the genome-wide analysis of REST ChIP-seq peaks from ENCODE. This ChIP-seq dataset has been generated using human cell lines (ENCODE Project Consortium, 2012). A given REST ChIP-seq peak from ENCODE was considered indicative of REST binding if the associated cluster score was higher than 850 in the 'wgEncodeRegTfbsClusteredV2' table of the UCSC Table Browser. Even high score peaks were filtered out if the peaks were not located within an annotated gene or maximum 6 kb upstream of the transcription start site of a gene. We refer to the mouse orthologs of these human REST-binding genes as 'high-confidence REST targets' (Table S2). This filtered set of REST-binding genes was considered applicable to the analysis of mouse data because the REST-binding RE1 motifs are conserved among vertebrates in 90% of the high-confidence REST target genes (Table S2). Potentially RFX-binding genes were identified in the mouse genome by searching for RFX1-binding motifs-like sequences in the 'Hub_186875_JasparTFBS' table using the UCSC Table Browser (Khan et al., 2018). The list of RFX1-binding motif-like sequences was filtered based on cluster score (cut-off: 400), conservation (>0.4 mean conservation score in the '60-vertebrate Basewise Conservation by PhyloP' table), and location (±300 bp from a transcription start site). Potential RFX1-binding motifs that overlapped with coding regions of genes were filtered out because conservation in these regions is more likely to indicate the non-neutral evolution of a protein-coding sequence than that of a potential regulatory motif. The utricular RNA-seq data were analyzed for potential differences in alternative splicing and polyA site selection using the JunctionSeq tool (Hartley and Mullikin, 2016). Adjusted p = 0.001 was selected as cut-off for significantly different exon usage in the JunctionSeq analysis. All potential splicing differences were tested by RT-PCR (see primers in Table S6). Uniprot keyword annotations of differentially expressed genes were identified using the DAVID software (Huang da et al., 2009). All genes expressed in E16 vestibular hair cells were used as the background gene set for the Uniprot keyword annotation analysis (Scheffer et al., 2015).

SAHA Treatment of Mice—SAHA was dissolved in DMSO and diluted 2-fold in Cremophor EL (Millipore). Just before the mice were injected, the DMSO/Cremphor EL solution of SAHA was diluted further in 0.9% NaCl. *Rest*$^{+/\Delta Ex4}$ and WT mice were injected

subcutaneously with 100 mg SAHA/kg body weight at P2, P4 and P5. In the control group, *Rest*$^{+/\Delta Ex4}$ and WT mice were injected with the vehicle solution only. At P6, the morphology of the organ of Corti and the extent of H4 acetylation were evaluated as described in the 'Immunofluorescence and Histochemistry' section. *Rest*$^{+/flEx4}$*;Rosa*$^{+/CreERT2}$ mice were injected with a mixture of SAHA (100 mg/kg body weight) and (Z)-4-hydroxytamoxifen (33 mg/kg body weight) at P7, P8, and P9. From P10 to P15, the same mice were injected with SAHA only (150 mg/kg body weight/day). In the control groups, *Rest*$^{+/flEx4}$*;Rosa*$^{+/CreERT2}$ mice were injected with (Z)-4-hydroxytamoxifen (33 mg/kg body weight/day at P7–P9) or vehicle only. WT mice were also treated with the same regimen of SAHA, (Z)-4-hydroxytamoxifen, and vehicle solution than *Rest*$^{+/flEx4}$*;Rosa*$^{+/CreERT2}$ mice. At P16, the ABR was measured to test the hearing thresholds of mice. Subsequently, the morphology of the organ of Corti or H4 acetylation was examined as described in the 'Immunofluorescence and Histochemistry' section.

QUANTIFICATION AND STATISTICAL ANALYSIS

Data are presented as individual data points, mean ± standard error of the mean (SEM), or median with minimum, maximum, 25th, and 75th percentile values, as indicated in the corresponding figure legends. The statistical methods applied are either indicated in the figure legend or described in the main text. Sample sizes were not determined *a priori*. RNA-seq data and Uniprot keyword annotations were analyzed using the DESeq2 software and the DAVID bioinformatics tool, respectively (see 'RNA Sequencing and Bioinformatics Analysis' section). scqRT-PCR data were analyzed using the SINGuLAR Analysis Toolset (Fluidigm) in R 3.0.2, as described in the 'Single Cell RT-PCR' section. All other data analyses were performed with GraphPad Prism version 7. For the datasets analyzed using GraphPad Prism, assumptions of normality were tested with the Shapiro-Wilk test and assumptions of equal variance with either the F-test (for two groups) or the Brown-Forsythe test (for three or more groups).

In cases where assumptions of normality and equal variance were not violated, parametric tests were used for the further analysis of datasets: the one-sample t test was used to compare the mean of one group to a hypothetical value; the unpaired Student's t test was used to compare the means of two groups; and one-way or two-way ANOVA was used (depending on the number of categorical independent variables) to compare the means of three or more groups. When ANOVA revealed significant findings, the Dunnett's post hoc test was used to compare the means of the test groups to the mean of a control group.

In the few cases where the assumption of equal variance (but not normality) was violated, Welch's t test was used to compare the means of two groups.

In cases where the assumption of normality (but not equal variance) was violated, non-parametric tests were used for the analysis of datasets: the one-sample Wilcoxon-signed rank test was used to compare the median of one group to a hypothetical value; and the Mann-Whitney test was used to compare the medians of two groups.

In cases where assumptions of both normality and equal variance were violated, one of two approaches was selected.

- Datasets presented in Figures 4E, 4F, and right panel of S6F were log2 transformed. Analyses of these log2 transformed data with the Shapiro-Wilk test and F-test revealed that assumptions of normality (but not equal variance) were violated. Therefore, following the log2 transformation the Mann-Whitney test was used to compare the medians of two groups.
- Datasets presented in Figure 6G were analyzed using a parametric test (i.e., two-way ANOVA) without data transformation. In this figure, ceiling effects led to violations of normality and equal variance assumptions. Specifically, thresholds of 32 kHz sound-evoked ABRs were higher than the maximum tested sound pressure level (i.e., 90 dB) in two groups of *Rest* exon 4 deficient mice. In the context of Figure 6G, these ceiling effects increased the probability of type II error (false negative) but not the type I error (false positive).

In figure panels where multiple one-sample tests or two-group tests were used, the Benjamini-Hochberg procedure was applied to limit the false discovery rate (FDR) at 0.05, as indicated in the relevant figure legends. For gene enrichment analysis, Fisher's exact test was used.

All reported p values are two-tailed, and $p < 0.05$ is considered statistically significant unless otherwise specified. Numbers of animals and biological replicates of assays (n) are reported in the figure legends if a statistical test was used or individual data points are not shown in the corresponding figure. Replicates for each experiment are outlined here:

- Figure 1C is representative of images from 3 independent assays. In each assay, one E15.5 mouse/genotype (utricle sample) and one P0 mouse/genotype (all other samples) were used. RNA was pooled from the left and right utricles of each mouse.
- Figures 1D and 1E represent data from 18 WT and 9 $Rest^{+/\Delta Ex4}$ mice.
- Figure 1F represents data from 12 WT and 10 $Rest^{+/\Delta Ex4}$ mice.
- Figures 1G and S2A are representative images of: 12 organs of Corti from 6 E17 WT mice; 8 organs of Corti from 4 P6 WT mice; 10 organs of Corti from 5 P12 WT mice; 8 organs of Corti from 4 E17 $Rest^{+/\Delta Ex4}$ mice; 10 organs of Corti from 5 P6 $Rest^{+/\Delta Ex4}$ mice; and 6 organs of Corti from 3 P12 $Rest^{+/\Delta Ex4}$ mice.
- Figure 1H is representative of images of: 6 utricles from 3 E16 WT mice; 8 utricles from 4 P6 WT mice; 10 utricles from 5 E16 $Rest^{+/\Delta Ex4}$ mice; and 14 utricles from 7 P6 $Rest^{+/\Delta Ex4}$ mice.
- Figure 1I represents data from 5 mice/group.
- Figures 1J and S3A are representative images of 10 inner ear preparations from 5 mice/group.
- Figure 2A represents data for the number of affected and unaffected subjects indicated in the LMG2 family pedigree in Figure 2B.
- Figure 3A represents data for two affected subjects from the LMG2 family and a control subject. The RT-PCR was repeated once (2 technical replicates).

- Figure 3C is representative of images from 4 independent assays.
- Figure 3G represents data from 4 independent assays.
- Figures 4A and 4B represent RNA-seq data from the number of tissue samples and mice described in the 'RNA Sequencing and Bioinformatics Analysis' section of Method Details.
- Figure 4D is representative of images of 14 utricles from 8 WT and 9 utricles from 6 *Rest*$^{+/\Delta Ex4}$ mice.
- Figures 4E and 4F represent data for 6 utricles from 3 mice/group. Individual data points represent the lengths of: 478 kinocilia in the WT E15 group; 177 kinocilia in the WT E16 group; 487 kinocilia in the *Rest*$^{+/\Delta Ex4}$ E15 group; 662 kinocilia in the *Rest*$^{+/\Delta Ex4}$ E16 group; 506 stereocilia bundles in the WT E15 group; 306 stereocilia bundles in the WT E16 group; 507 stereocilia bundles in the *Rest*$^{+/\Delta Ex4}$ E15 group; and 458 stereocilia bundles in the *Rest*$^{+/\Delta Ex4}$ E16 group.
- Figure 5A: Left panel is representative of images from 3 independent assays (one mouse/time point in each assay). Middle and right panels are representative of images from 2 independent assays (one sample/time point in each assay; 6–10 hearing or balance organs from 3–5 mice were pooled for each sample).
- Figure 5C is representative of images of 6 cortical sections from 3 mice/time point (2 cortical sections/mouse/time point).
- Figure 5D is representative of images of 10–12 inner ear sections from 3 mice/time point.
- Figure 5E represents data from 3 mice/group. 1–3 organ of Corti-containing areas were analyzed in each section. Data points indicate the intensity of EGFP signal in: 138 cortical neurons at P0; 34 cortical neurons at P16; 58 OHCs at P0; 62 OHCs at P6; 44 OHCs at P16; 23 IHCs at P0; 21 IHCs at P6; and 26 IHCs at P16.
- Figure 5F represents data from: 159 non-HCs isolated from 5 P1 mice; 63 non-HCs isolated from 4 P7 mice; 20 OHCs isolated from 5 P1 mice; 19 OHCs isolated from 4 P7 mice; 9 IHCs isolated from 3 P1 mice; and 4 IHCs isolated from 2 P7 mice.
- Figures 5G and 5H represent data from: 10 non-HCs isolated from 3 P1 mice; 10 non-HCs isolated from 3 P7 mice; 8 OHCs isolated from 3 P1 mice; 10 OHCs isolated from 3 P7 mice; 4 IHCs isolated from 3 P1 mice; and 4 IHCs isolated from 2 P7 mice.
- Figure 6A is representative of images of: 5 non-treated WT cultures; 4 non-treated *Rest*$^{+/\Delta Ex4}$ cultures; and 5 FK228-treated *Rest*$^{+/\Delta Ex4}$ cultures. Within a treatment group, each culture was derived from a different mouse.
- Figure 6B represents data from: 5 non-treated WT cultures; 4 non-treated *Rest*$^{+/\Delta Ex4}$ cultures; 5 FK228-treated *Rest*$^{+/\Delta Ex4}$ cultures; 4 SAHA-treated *Rest*$^{+/\Delta Ex4}$

cultures; and 4 Merck60-treated *Rest*$^{+/\Delta Ex4}$ cultures. Within a treatment group, each culture was derived from a different mouse.

- Figures 6C, 6D, and S6B represent images and data from: 4 non-treated WT mice; 4 non-treated *Rest*$^{+/\Delta Ex4}$ mice; and 6 SAHA-treated *Rest*$^{+/\Delta Ex4}$ mice. In Figure 6D, the hair cell counts are the average for the two ears of each mouse.
- Figures 6E and S6D represent data and images from 3 organ cultures/group (one organ culture/mouse/group).
- Figures 6F and S6E represent data and images from 3 mice/group. Hair cell counts were averaged from the two cochleas of each mouse.
- Figures 6G represents data from 8 mice in the '*Rest*$^{+/flEx4}$;*Rosa*$^{+/CreERT2}$ + T + SAHA' group and 7 mice/group in all other groups. ABR thresholds were determined for each mouse at each sound frequency indicated in the figure.
- Figure S1B is representative of images from 2 independent assays. DNA from 2 WT mice and 3 *Rest*$^{+/flNeoEx4}$ mice was analyzed in these assays (one DNA sample/mouse).
- Figure S1C is representative of images from 3 independent assays. RNA from 3 WT and 4 *Rest*$^{flEx4/flEx4}$ mice was analyzed in the 3 assays (one RNA sample/mouse were analyzed).
- Figure S1D represents data from 3 WT and 4 *Rest*$^{flEx4/flEx4}$ mice.
- Figure S1E is representative of images from 3 independent assays (one mouse/genotype/assay).
- Figure S1F represents data from 4 mice/genotype/time point.
- Figure S1G is representative of images of 4 organs of Corti from 2 mice/genotype.
- Figure S1H is representative of images of 4 utricles from 2 mice/genotype.
- Figure S1I is representative of images of 8 organs of Corti and 8 utricles from 4 mice.
- Figure S2B is representative of images of: 6 utricles and 6 anterior cristae ampullaris from 3 E16 WT mice; 8 utricles and 8 anterior cristae ampullaris from 4 P6 WT mice; 10 utricles and 10 anterior cristae ampullaris from 5 E16 *Rest*$^{+/\Delta Ex4}$ mice; and 14 utricles and 14 anterior cristae ampullaris from 7 P6 *Rest*$^{+/\Delta Ex4}$ mice.
- Figures S2C and S2D represent data from the number of inner ears and mice indicated in the legend of Figure S2.
- Figure S3B is representative of images from 2 independent assays. In each assay, DNA samples from 2 WT, 3 *Rest*$^{+/flEx4}$;*Rosa*$^{+/CreERT2}$, and 3 '*Rest*$^{+/flEx4}$;*Rosa*$^{+/CreERT2}$ + T' mice were analyzed.
- Figure S3C is representative of images of 6 organs of Corti of 3 mice/genotype.

- Figure S3D is representative of images of 4 solvent-incubated organ cultures and 5 Z-DEVD-FMK-incubated organ cultures (one culture/mouse/incubation condition).
- Figure S3E represents data from: 4 organ cultures incubated with solvent; 5 organ cultures incubated with Z-DEVD-FMK; and 5 organ cultures incubated with Z-VAD-FMK (one organ culture/mouse/incubation condition).
- Figure S3F is representative of images of 40 brain sections from 2 WT mice and 91 brain sections from 4 $Rest^{+/\Delta Ex4}$ mice.
- Figure S3G is representative of images of 16 cortical sections from 4 mice/genotype (4 sections/mouse).
- Figure S3H represents data from 4 mice/genotype (4 sections/mouse were analyzed).
- Figure S3I represents data from 3 mice/genotype (2 sections/mouse were analyzed).
- Figure S3J is representative of images of 61 sections from 4 WT mice and 58 sections from 4 $Rest^{+/\Delta Ex4}$ mice.
- Figure S3K represents data from: 13 WT mice at P30; 3 WT mice at P130; 4 $Rest^{+/\Delta Ex4}$ mice at P30; and 3 $Rest^{+/\Delta Ex4}$ mice at P130.
- Figure S3M is representative of images of 3 technical replicates/primer pair. One human RNA sample per organ was used.
- Figure S3N is representative of images from 2 independent assays.
- Figure S4A is representative of a single assay/primer pair.
- Figure S4C represents data from 3 mice/genotype (RNA was pooled from the left and right utricles and saccules of each mouse).
- Figure S4G represents data from 5 independent assays.
- Figure S4H represents data from 3 mice/genotype at each time point (RNA was pooled from the left and right utricles and saccules of each mouse).
- Figure S4I is representative of images of 4 utricles and 4 saccules from 2 '$Rest^{+/flEx4};Rosa^{+/CreERT2}$ –T' mice, and of 6 utricles and 6 saccules from 3 '$Rest^{+/flEx4};Rosa^{+/CreERT2}$ + T' mice.
- Figure S4J is representative of images of 6 utricles from 3 mice at P0 and 10 utricles from 5 mice at P16.
- Figure S5A represents data from 3 independent assays/treatment conditions.
- Figure S5B is representative of images of: 5 non-treated WT cultures; 3 FK228-treated WT cultures; 3 SAHA-treated WT cultures; 3 Merck60-treated WT cultures; 4 non-treated $Rest^{+/\Delta Ex4}$ cultures; 5 FK228-treated $Rest^{+/\Delta Ex4}$ cultures; 4 SAHA-treated $Rest^{+/\Delta Ex4}$ cultures; and 4 Merck60-treated $Rest^{+/\Delta Ex4}$ cultures. Within a treatment group, each culture was derived from a different mouse.

- Figure S5E represents data from 3 independent samples/treatment conditions (6–8 organ cultures from 3–4 mice were pooled to obtain a single sample).
- Figure S6A represents data from 3 organ cultures/group (one organ culture/mouse/group).
- Figure S6C is representative of images from 2 independent assays. DNA was isolated from 4 organ cultures (derived from 2 mice) to obtain a single sample. In the 2 assays, 2 samples per treatment condition were analyzed.
- Figure S6F represents data from: 36 OHCs from 2 vehicle-injected mice (left panel); 40 OHCs from 2 SAHA-injected mice (left panel); 90 OHCs from 4 vehicle-injected mice (right panel); and 48 OHCs from 4 SAHA-injected mice (right panel).

Supplementary Material

Refer to Web version on PubMed Central for supplementary material.

ACKNOWLEDGMENTS

We thank the LMG2 family for participation in this study. We thank Susan Wiechert for technical assistance; Jian Zuo for providing the *Gfi1*$^{+/Cre}$ mouse; Dennis Drayna, Doris Wu, and Christine Blaumueller for critical review of the manuscript; and Stephen Elledge for providing REST-encoding plasmids. This project was supported by grants from the NIH (R01DC010152 and R01DC014953 to B.B.) and in part by funds from the NIDCD Division of Intramural Research/NIH (DC000048 to T.B.F., DC000086 to R.J.M and DC000059 to M.W.K). This work utilized computational resources of the NIH HPC Biowulf cluster (http://hpc.nih.gov).

REFERENCES

Ballas N, Grunseich C, Lu DD, Speh JC, and Mandel G (2005). REST and its corepressors mediate plasticity of neuronal gene chromatin throughout neurogenesis. Cell 121, 645–657. [PubMed: 15907476]

Bayram Y, White JJ, Elcioglu N, Cho MT, Zadeh N, Gedikbasi A, Palanduz S, Ozturk S, Cefle K, Kasapcopur O, et al. (2017). REST final–exon–truncating mutations cause hereditary gingival fibromatosis. Am. J. Hum. Genet 101, 149–156. [PubMed: 28686854]

Burns JC, Kelly MC, Hoa M, Morell RJ, and Kelley MW (2015). Single–cell RNA–Seq resolves cellular complexity in sensory organs from the neonatal inner ear. Nat. Commun 6, 8557. [PubMed: 26469390]

Cai T, Jen HI, Kang H, Klisch TJ, Zoghbi HY, and Groves AK (2015). Characterization of the transcriptome of nascent hair cells and identification of direct targets of the Atoh1 transcription factor. J. Neurosci 35, 5870–5883. [PubMed: 25855195]

Calarco JA, Superina S, O'Hanlon D, Gabut M, Raj B, Pan Q, Skalska U, Clarke L, Gelinas D, van der Kooy D, et al. (2009). Regulation of vertebrate nervous system alternative splicing and development by an SR–related protein. Cell 138, 898–910. [PubMed: 19737518]

Chen ZF, Paquette AJ, and Anderson DJ (1998). NRSF/REST is required in vivo for repression of multiple neuronal target genes during embryogenesis. Nat. Genet 20, 136–142. [PubMed: 9771705]

Chong JA, Tapia–Ramirez J, Kim S, Toledo–Aral JJ, Zheng Y, Boutros MC, Altshuller YM, Frohman MA, Kraner SD, and Mandel G (1995). REST: a mammalian silencer protein that restricts sodium channel gene expression to neurons. Cell 80, 949–957. [PubMed: 7697725]

Dobin A, Davis CA, Schlesinger F, Drenkow J, Zaleski C, Jha S, Batut P, Chaisson M, and Gingeras TR (2013). STAR: ultrafast universal RNA–seq aligner. Bioinformatics 29, 15–21. [PubMed: 23104886]

ENCODE Project Consortium (2012). An integrated encyclopedia of DNA elements in the human genome. Nature 489, 57–74. [PubMed: 22955616]

Farley FW, Soriano P, Steffen LS, and Dymecki SM (2000). Widespread recombinase expression using FLPeR (flipper) mice. Genesis 28, 106–110. [PubMed: 11105051]

Ganesan A (2015). Macrocyclic inhibitors of zinc–dependent histone deacetylases (HDACs) In Macrocycles in Drug Discovery, Levin J, ed. (Royal Society of Chemistry), pp. 109–140.

Gao Z, Ure K, Ding P, Nashaat M, Yuan L, Ma J, Hammer RE, and Hsieh J (2011). The master negative regulator REST/NRSF controls adult neurogenesis by restraining the neurogenic program in quiescent stem cells. J. Neurosci 31, 9772–9786. [PubMed: 21715642]

Gong S, Zheng C, Doughty ML, Losos K, Didkovsky N, Schambra UB, Nowak NJ, Joyner A, Leblanc G, Hatten ME, et al. (2003). A gene expression atlas of the central nervous system based on bacterial artificial chromosomes. Nature 425, 917–925. [PubMed: 14586460]

Hameyer D, Loonstra A, Eshkind L, Schmitt S, Antunes C, Groen A, Bindels E, Jonkers J, Krimpenfort P, Meuwissen R, et al. (2007). Toxicity of ligand–dependent Cre recombinases and generation of a conditional Cre deleter mouse allowing mosaic recombination in peripheral tissues. Physiol. Genomics 31, 32–41. [PubMed: 17456738]

Hanson JE, La H, Plise E, Chen YH, Ding X, Hanania T, Sabath EV, Alexandrov V, Brunner D, Leahy E, et al. (2013). SAHA enhances synaptic function and plasticity in vitro but has limited brain availability in vivo and does not impact cognition. PLoS One 8, e69964. [PubMed: 23922875]

Hartley SW, and Mullikin JC (2016). Detection and visualization of differential splicing in RNA–Seq data with JunctionSeq. Nucleic Acids Res. 44, e127. [PubMed: 27257077]

Huang DW, Sherman BT, and Lempicki RA (2009). Systematic and integrative analysis of large gene lists using DAVID bioinformatics resources. Nat. Protoc 4, 44–57. [PubMed: 19131956]

Karolchik D, Hinrichs AS, Furey TS, Roskin KM, Sugnet CW, Haussler D, and Kent WJ (2004). The UCSC Table Browser data retrieval tool. Nucleic Acids Res 32, D493–496. [PubMed: 14681465]

Khan A, Fornes O, Stigliani A, Gheorghe M, Castro–Mondragon JA, van der Lee R, Bessy A, Chèneby J, Kulkarni SR, Tan G, et al. (2018). JASPAR 2018: update of the open–access database of transcription factor binding profiles and its web framework. Nucleic Acids Res 46, D260–D266. [PubMed: 29140473]

Konsoula R, and Jung M (2008). In vitro plasma stability, permeability and solubility of mercaptoacetamide histone deacetylase inhibitors. Int. J. Pharm 361, 19–25. [PubMed: 18562136]

Lewandoski M, Meyers EN, and Martin GR (1997). Analysis of Fgf8 gene function in vertebrate development. Cold Spring Harb. Symp. Quant. Biol 62, 159–168. [PubMed: 9598348]

Love MI, Huber W, and Anders S (2014). Moderated estimation of fold change and dispersion for RNA–seq data with DESeq2. Genome Biol. 15, 550. [PubMed: 25516281]

Magin A, Lietz M, Cibelli G, and Thiel G (2002). RE–1 silencing transcription factor–4 (REST4) is neither a transcriptional repressor nor a de–repressor. Neurochem. Int 40, 195–202. [PubMed: 11741002]

Mahamdallie SS, Hanks S, Karlin KL, Zachariou A, Perdeaux ER, Ruark E, Shaw CA, Renwick A, Ramsay E, Yost S, et al. (2015). Mutations in the transcriptional repressor REST predispose to Wilms tumor. Nat. Genet 47, 1471–1474. [PubMed: 26551668]

Mandel G, Fiondella CG, Covey MV, Lu DD, Loturco JJ, and Ballas N (2011). Repressor element 1 silencing transcription factor (REST) controls radial migration and temporal neuronal specification during neocortical development. Proc. Natl. Acad. Sci. USA 108, 16789–16794. [PubMed: 21921234]

Mann BS, Johnson JR, Cohen MH, Justice R, and Pazdur R (2007). FDA approval summary: vorinostat for treatment of advanced primary cutaneous T–cell lymphoma. Oncologist 12, 1247–1252. [PubMed: 17962618]

Manojlovic Z, Earwood R, Kato A, Stefanovic B, and Kato Y (2014). RFX7 is required for the formation of cilia in the neural tube. Mech. Dev 132, 28–37. [PubMed: 24530844]

McGann JC, Oyer JA, Garg S, Yao H, Liu J, Feng X, Liao L, Yates JR, 3rd, and Mandel G (2014). Polycomb–and REST–associated histone deacetylases are independent pathways toward a mature neuronal phenotype. Elife 3, e04235. [PubMed: 25250711]

Methot JL, Chakravarty PK, Chenard M, Close J, Cruz JC, Dahlberg WK, Fleming J, Hamblett CL, Hamill JE, Harrington P, et al. (2008). Exploration of the internal cavity of histone deacetylase (HDAC) with selective HDAC1/HDAC2 inhibitors (SHI–1:2). Bioorg. Med. Chem. Lett 18, 973–978. [PubMed: 18182289]

Nakano Y, Jahan I, Bonde G, Sun X, Hildebrand MS, Engelhardt JF, Smith RJ, Cornell RA, Fritzsch B, and Banfi B (2012). A mutation in the Srrm4 gene causes alternative splicing defects and deafness in the Bronx waltzer mouse. PLoS Genet. 8, e1002966. [PubMed: 23055939]

Nechiporuk T, McGann J, Mullendorff K, Hsieh J, Wurst W, Floss T, and Mandel G (2016). The REST remodeling complex protects genomic integrity during embryonic neurogenesis. Elife 5, e09584. [PubMed: 26745185]

Palm K, Metsis M, and Timmusk T (1999). Neuron–specific splicing of zinc finger transcription factor REST/NRSF/XBR is frequent in neuroblastomas and conserved in human, mouse and rat. Brain Res. Mol. Brain Res 72, 30–39. [PubMed: 10521596]

Paquette AJ, Perez SE, and Anderson DJ (2000). Constitutive expression of the neuron–restrictive silencer factor (NRSF)/REST in differentiating neurons disrupts neuronal gene expression and causes axon pathfinding errors in vivo. Proc. Natl. Acad. Sci. USA 97, 12318–12323. [PubMed: 11050251]

Peters LM, Fridell RA, Boger ET, San Agustin TB, Madeo AC, Griffith AJ, Friedman TB, and Morell RJ (2008). A locus for autosomal dominant progressive non–syndromic hearing loss, DFNA27, is on chromosome 4q12–13.1. Clin. Genet 73, 367–372. [PubMed: 18279434]

Raj B, Irimia M, Braunschweig U, Sterne–Weiler T, O'Hanlon D, Lin ZY, Chen GI, Easton LE, Ule J, Gingras AC, et al. (2014). A global regulatory mechanism for activating an exon network required for neurogenesis. Mol. Cell 56, 90–103. [PubMed: 25219497]

Raj B, O'Hanlon D, Vessey JP, Pan Q, Ray D, Buckley NJ, Miller FD, and Blencowe BJ (2011). Cross-regulation between an alternative splicing activator and a transcription repressor controls neurogenesis. Mol. Cell 43, 843–850. [PubMed: 21884984]

Scheffer DI, Shen J, Corey DP, and Chen ZY (2015). Gene expression by mouse inner ear hair cells during development. J. Neurosci 35, 6366–6380. [PubMed: 25904789]

Schoenherr CJ, and Anderson DJ (1995). The neuron–restrictive silencer factor (NRSF): a coordinate repressor of multiple neuron–specific genes. Science 267, 1360–1363. [PubMed: 7871435]

Suzuki M, Yamasoba T, and Kaga K (1998). Development of the blood–labyrinth barrier in the rat. Hear Res. 116, 107–112. [PubMed: 9508033]

Wagner FF, Zhang YL, Fass DM, Joseph N, Gale JP, Weiwer M, McCarren P, Fisher SL, Kaya T, Zhao WN, et al. (2015). Kinetically selective inhibitors of histone deacetylase 2 (HDAC2) as cognition enhancers. Chem. Sci 6, 804–815. [PubMed: 25642316]

Wallis D, Hamblen M, Zhou Y, Venken KJ, Schumacher A, Grimes HL, Zoghbi HY, Orkin SH, and Bellen HJ (2003). The zinc finger transcription factor Gfi1, implicated in lymphomagenesis, is required for inner ear hair cell differentiation and survival. Development 130, 221–232. [PubMed: 12441305]

Westbrook TF, Hu G, Ang XL, Mulligan P, Pavlova NN, Liang A, Leng Y, Maehr R, Shi Y, Harper JW, et al. (2008). SCFbeta–TRCP controls oncogenic transformation and neural differentiation through REST degradation. Nature 452, 370–374. [PubMed: 18354483]

Yang H, Gan J, Xie X, Deng M, Feng L, Chen X, Gao Z, and Gan L (2010). Gfi1–Cre knock–in mouse line: A tool for inner ear hair cell–specific gene deletion. Genesis 48, 400–406. [PubMed: 20533399]

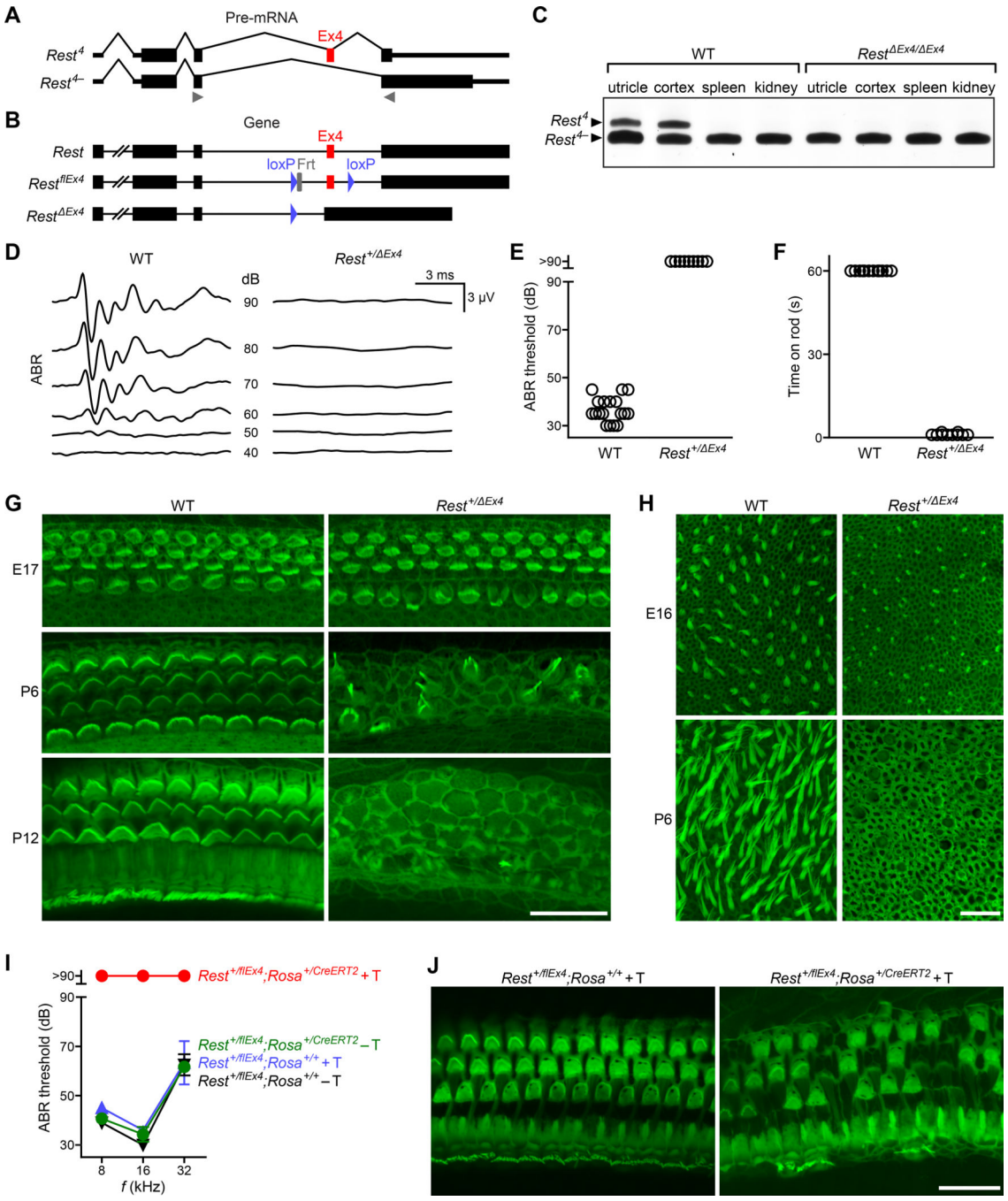

Figure 1. *Rest* Exon 4 Is Critical for Hearing in Mice

(A) Schematic of exon-intron structures of *Rest* isoforms, illustrating differences in lengths of reading frames between the exon 4-containing (*Rest*^{4}) and exon 4-omitting (*Rest*$^{4-}$) splice forms. Constitutively spliced exons (black rectangles), exon 4 (Ex4, red), and UTRs (thin rectangles) are indicated. Tented lines represent joining of exons in maturing pre-mRNA. Gray arrowheads show positions of RT-PCR primers used in experiments depicted in (C).

(B) Schematic of wild-type (WT) *Rest*, an exon 4-floxed form of *Rest* (*Rest*^{flEx4}), and an exon 4-deleted form of *Rest* (*Rest*$^{\Delta Ex4}$). Exons and introns are indicated as in (A). Blue and gray symbols represent loxP and Frt sites, respectively.

(C) RT-PCR analysis of exon 4 splicing in indicated tissues of WT mice and mutant mice homozygous for the dominant *Rest*$^{\Delta Ex4}$ allele. RNA was isolated at E15.5 (utricle) and P0 (other tissues). Spleen and kidney are shown as examples of non-neural tissues.

(D) Representative ABR waveforms for WT and *Rest*$^{+/\Delta Ex4}$ mice at P28. Broadband click stimuli were applied at sound pressure levels indicated in decibels.

(E) Thresholds of broadband click-evoked ABRs of WT and *Rest*$^{+/\Delta Ex4}$ mice at P28. Each symbol represents value for a single mouse.

(F) Time spent on a horizontal rod before falling for WT and *Rest*$^{+/\Delta Ex4}$ mice at P21–P28. Maximal duration of the assay was 60 s.

(G and H) Organ of Corti (G) and utricle (H) preparations from WT and *Rest*$^{+/\Delta Ex4}$ mice at the indicated developmental stages, stained with phalloidin-Alexa488 to visualize F-actin-rich structures, including stereocilia and cell-cell borders. Scale bars, 20 μm.

(I) ABR thresholds of P70–P80 control (*Rest*$^{+/flEx4}$;*Rosa*$^{+/+}$) and *Rest*$^{+/flEx4}$;*Rosa*$^{+/CreERT2}$ mice treated with tamoxifen (+T) or solvent (–T) from P40 to P47. Pure-tone stimuli were applied at frequencies indicated (n = 5 mice/group). Values are mean ± SEM.

(J) F-actin-stained organ of Corti preparations from control (*Rest*$^{+/flEx4}$;*Rosa*$^{+/+}$) and *Rest*$^{+/flEx4}$;*Rosa*$^{+/CreERT2}$ mice at P79, following treatment with tamoxifen from P40 to P47. Scale bar, 20 μm.

See also Figures S1, S2, and S3.

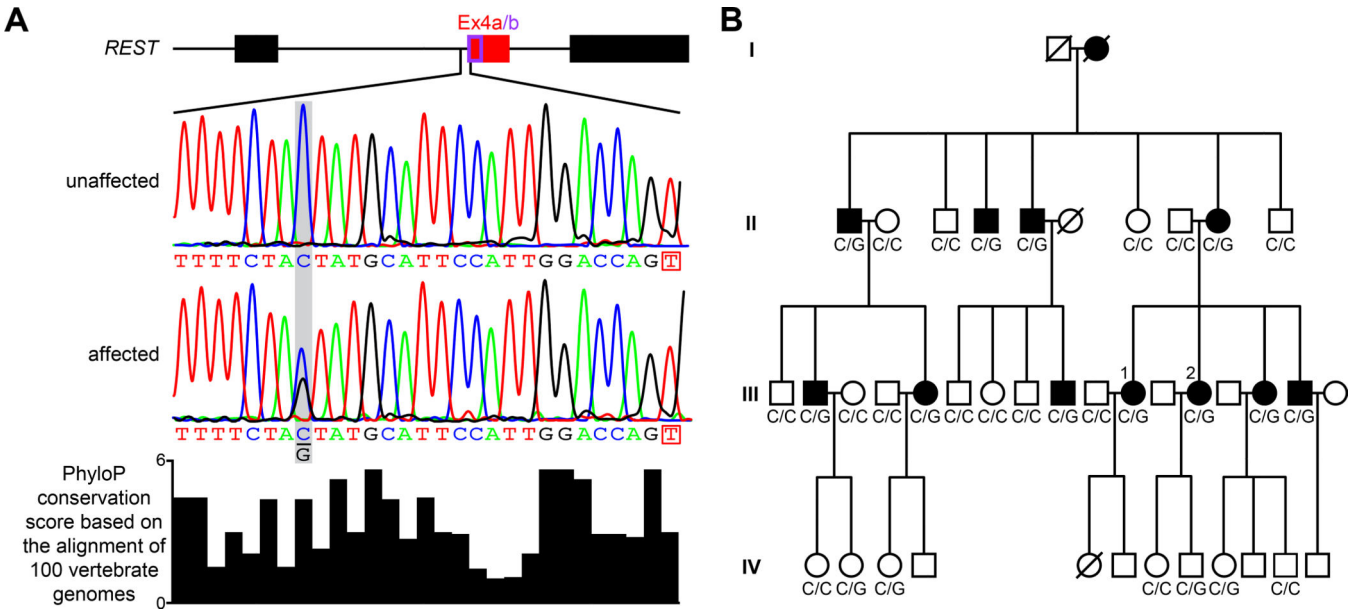

Figure 2. *DFNA27* Contains an Intronic C > G Variant near *REST* Exon 4

(A) Location and conservation of *REST* region containing a C > G variant in family LMG2. Top: schematic of exon-intron structure of *REST* from exon 3 to exon 5 is shown. Rectangles indicate exons 3 and 5 (black), exon 4a (red), and exon 4b (purple outline). Introns are shown as horizontal lines. Middle: chromatograms depict genomic sequences upstream of exon 4a/b in an unaffected and an affected heterozygous subject. In the affected subject, the wild-type C nucleotide in intron 3 of *REST* is replaced by a G (gray shading). First base of exon 4a/b is boxed. Bottom: vertebrate PhyloP conservation score is shown. (B) Pedigree of LMG2 family, showing cosegregation of progressive hearing loss with intronic C > G variant of *REST*. Filled symbols represent individuals with hearing loss; hearing data are not available for generation IV. Letters beneath symbols indicate nucleotides 21 bases upstream of *REST* exon 4 in the individual. Arabic numerals identify subjects whose RNA was analyzed (Figure 3A).

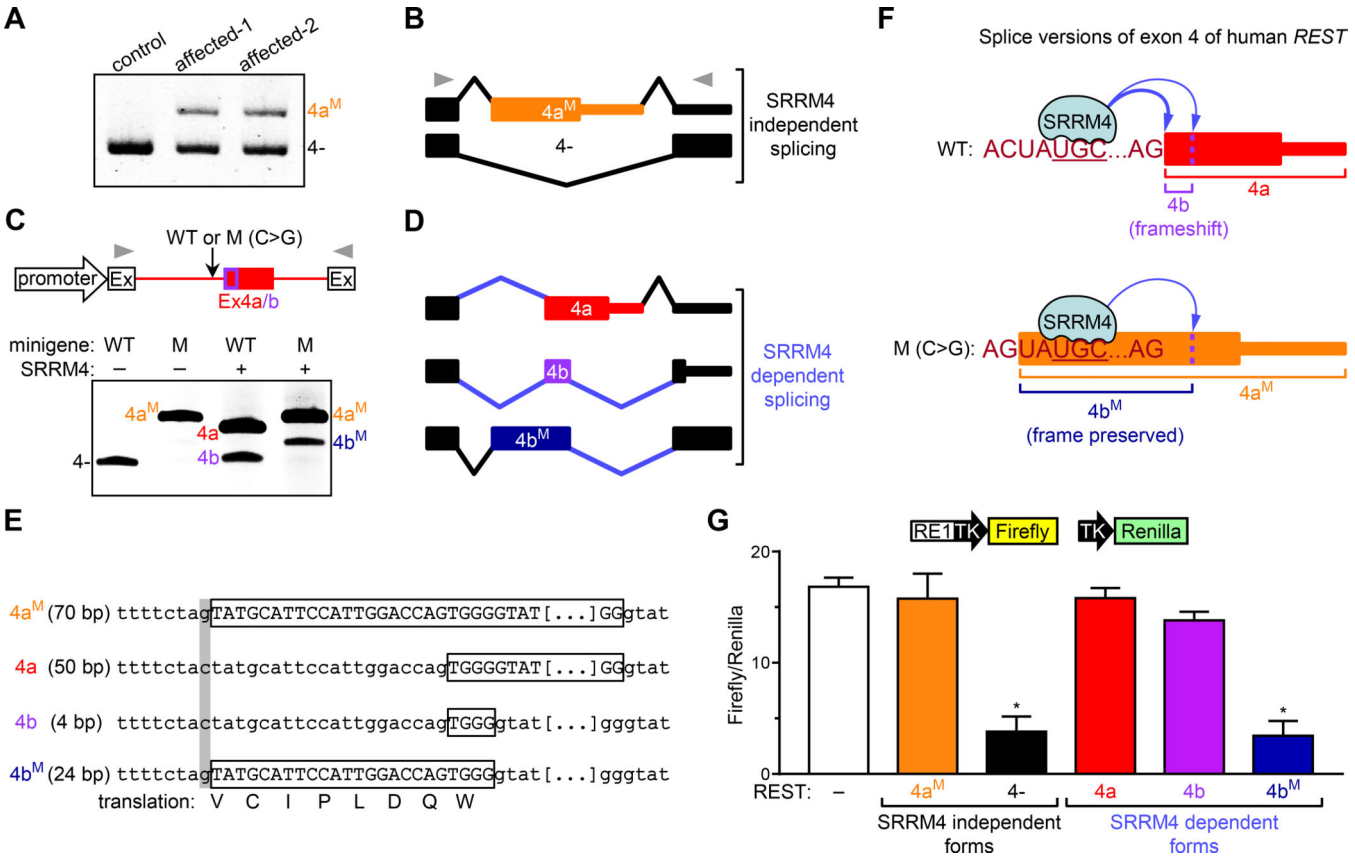

Figure 3. C > G *DFNA27* Variant Prevents Alternative Splicing-Dependent REST Inactivation

(A) RT-PCR for the detection of *REST* splice forms in blood cells from two affected subjects (indicated by numbers in Figure 2B) and a control subject. Locations of PCR primers are shown in (B) (gray arrowheads). $4a^M$ and 4- indicate detected mutant and wild-type (WT) splice forms, respectively.

(B) Schematic of splice site selection in $4a^M$ and 4- splice forms shown in (A). SRRM4-independent splicing refers to a lack of SRRM4 in blood cells. Constitutively spliced exons 3 and 5 (black rectangles), exon $4a^M$ (orange), and UTRs (thin rectangles) are indicated. Tented lines represent joining of exons in pre-mRNA.

(C) RT-PCR testing of effect of C > G variant on splicing of exons 4a/b in HEK293 cells co-transfected with a *REST* minigene and an SRRM4-encoding plasmid or empty vector. Top: schematic of minigenes is shown, with constitutively spliced exons (Ex) flanking WT or *DFNA27* (mutant [M]) version of exon 4a/b (Ex4a/b)-containing *REST* segment. Minigene promoter, positions of RT-PCR primers (arrowheads), and mutation site (vertical arrow) are indicated. Bottom: 4-, 4a, and 4b represent detected WT splice forms; $4a^M$ and $4b^M$ represent detected mutant splice forms.

(D) Schematic of SRRM4-dependent splice site selection (blue lines) in 4a, 4b, and $4b^M$ splice forms shown in (C).

(E) Sequences (boxed) and lengths (bp) of indicated exon 4 splice forms. Gray shading indicates site of mutation. Translation line shows amino acids encoded by exon $4b^M$.

(F) Illustrations of effects of SRRM4 on splice sites (curved arrows) and reading frames in transcripts encoded by WT and *DFNA27* (mutant [M]) *REST* forms. Vertical dotted lines

indicate SRRM4-dependent splice donor site. UGC core of SRRM4-binding motif is underlined.

(G) Expression levels of REST binding site (RE1)-containing reporter gene in Neuro2a cells transfected with empty vector (–) or indicated *REST* splice form. Schematic at top shows compositions of Firefly reporter and Renilla control constructs. Values are mean ± SEM; n = 4 independent assays; one-way ANOVA, $p < 0.0001$; post hoc Dunnett's test, *$p < 0.0001$ (control group, –). TK, thymidine kinase gene promoter.

See also Figure S3.

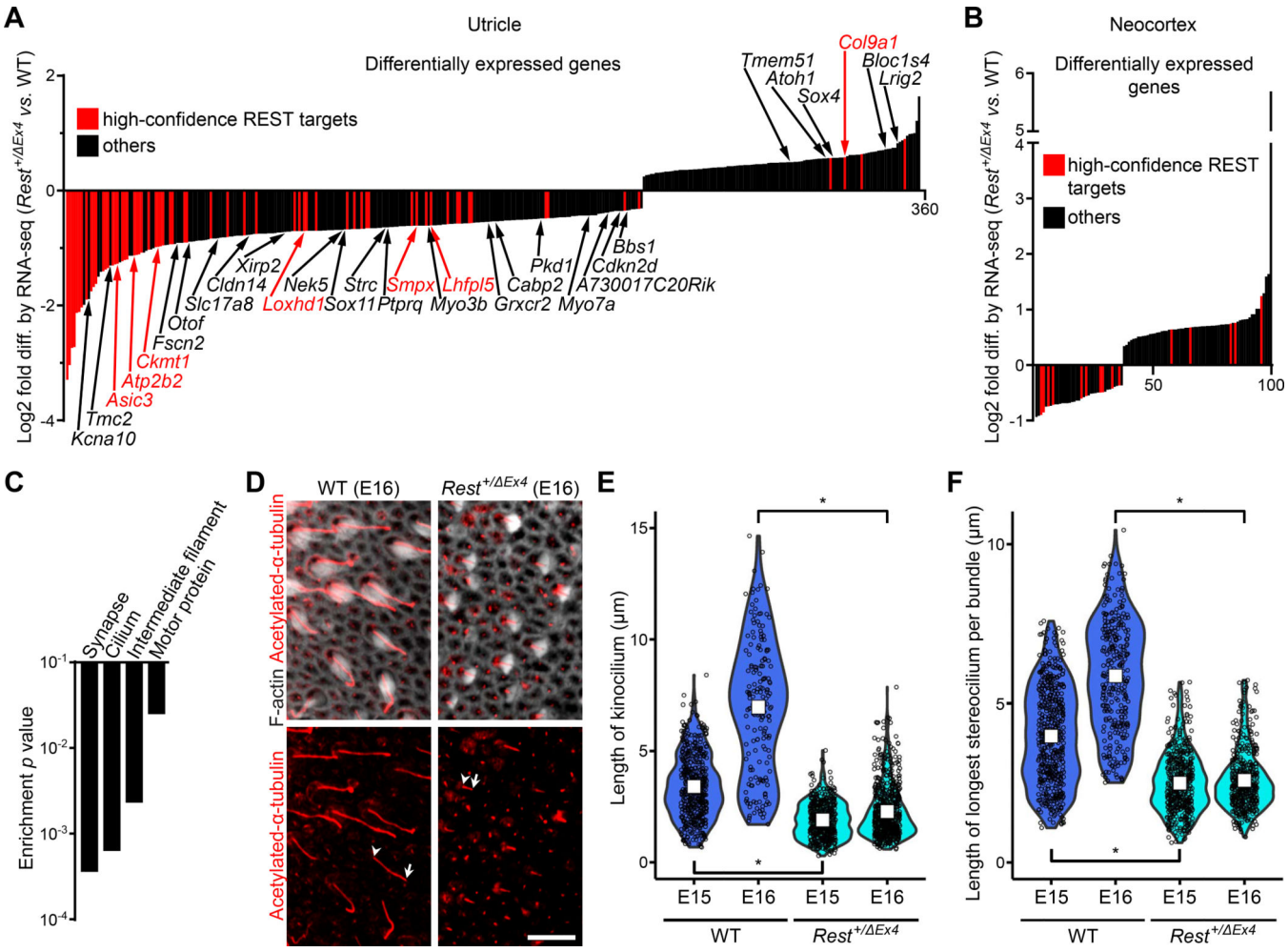

Figure 4. Genomic Deletion of Exon 4 of Mouse *Rest* Is Associated with Reduced Expression of Many Hearing-Related Genes

(A) Differences in gene expression between utricles of WT and *Rest*$^{+/\Delta Ex4}$ mice at E15.5. Red bars indicate high-confidence REST target genes. Arrows and names indicate differences in expression levels of genes known to be important for hearing or balance. Names of all differentially expressed genes are listed in Table S1.

(B) Differences in gene expression between the neocortices of WT and *Rest*$^{+/\Delta Ex4}$ mice at E15.5. Color coding is same as in (A); gene names are listed in Table S4.

(C) Enrichment of Uniprot keyword annotations in set of genes differentially expressed in the *Rest*$^{+/\Delta Ex4}$ versus WT mouse utricle.

(D) Representative images of stereocilia (F-actin staining, white bundles) and kinocilia (acetylated α-tubulin immunostaining, red strips) in utricles of *Rest*$^{+/\Delta Ex4}$ and WT mice at E16. For two kinocilia, tip (arrow) and base (arrowhead) are indicated in lower panels. Scale bar, 10 μm.

(E and F) Violin plots of lengths of kinocilia (E) and maximum lengths of stereocilia bundles (F) in WT and *Rest*$^{+/\Delta Ex4}$ mouse utricular hair cells at E15 and E16. Each circle represents one kinocilium (E) or longest stereocilium (F) of a hair cell (pooled data from 6

utricles of 3 mice/group). White rectangles indicate means. Mann-Whitney test, false discovery rate (FDR) adjusted, *$p < 0.0001$.
See also Figure S4, Tables S1, S2, S3, and S4.

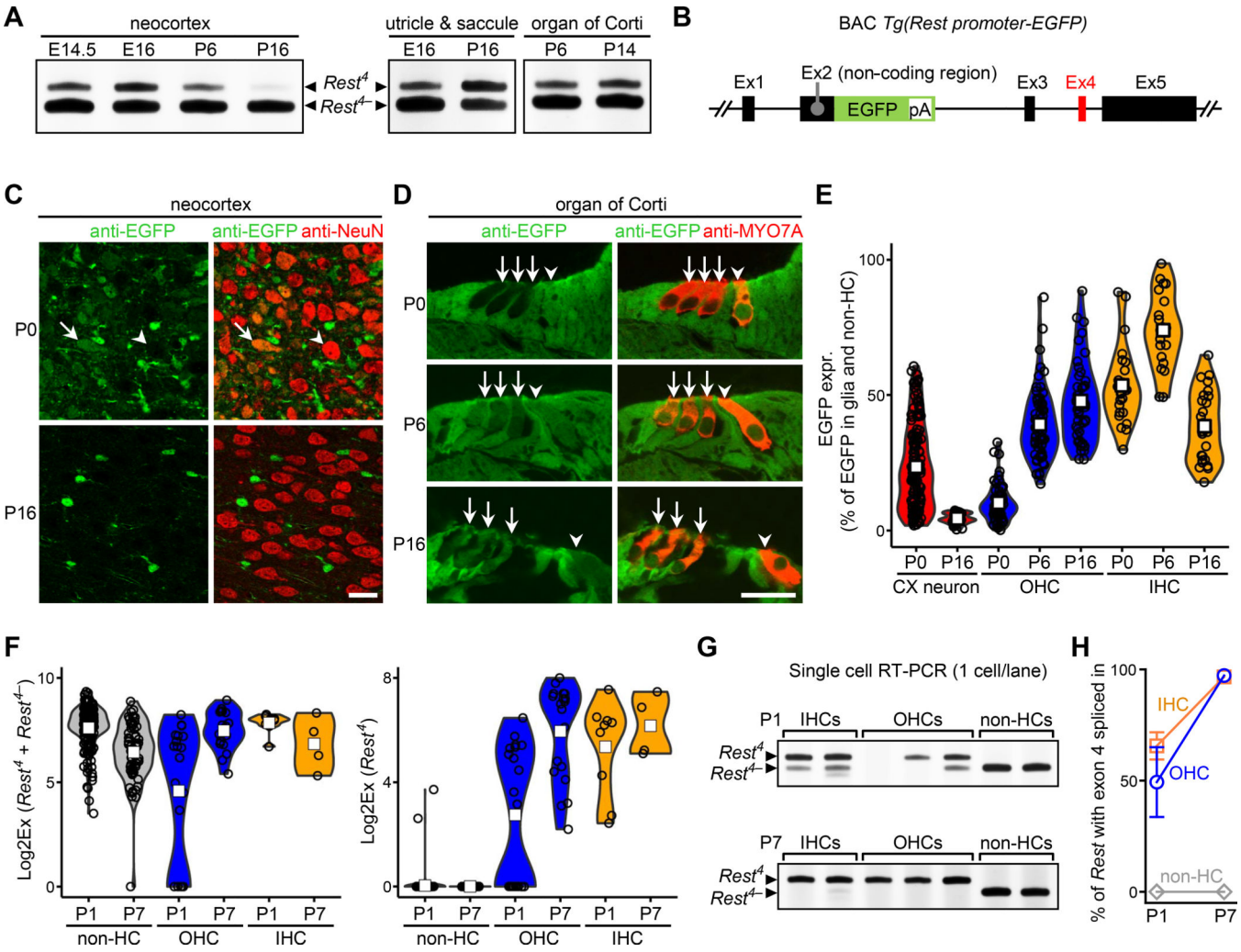

Figure 5. Contributions of Alternative Splicing and Transcriptional Silencing to the Downregulation of REST Activity Differ in Hair Cells and Cortical Neurons

(A) RT-PCR analysis of *Rest* exon 4 splicing in indicated tissues of WT mice.

(B) Schematic of BAC transgene engineered for quantification of *Rest* promoter activity. Transgene contains an EGFP reporter (green box) immediately downstream of *Rest* start codon. pA, polyadenylation signal. Exons and introns of *Rest* are indicated as in Figure 1B.

(C) EGFP (green) and NeuN (red) immunofluorescence in cortical sections from *Tg(Rest promoter-EGFP)* mice at P0 and P16. Examples of cells that are NeuN-positive and either EGFP positive (arrow) or negative (arrowhead) are shown. Scale bar, 20 μm.

(D) EGFP (green) and MYO7A (red) immunofluorescence in cochlear sections from *Tg(Rest promoter-EGFP)* mice at P0, P6, and P16. Arrows, OHCs; arrowheads, IHCs. Scale bar, 20 μm.

(E) Violin plot of *Tg(Rest promoter-EGFP)* expression in cortical (CX) neurons, OHCs, and IHCs at the indicated times, as determined by immunoflourescence. EGFP signal was quantified as the percentage of that in non-neuronal cells and non-hair cells in the same sections. Each circle represents an individual cell. White rectangles indicate means.

(F) Violin plot of total *Rest* expression (left plot) and $Rest^{\Delta 4}$ expression (right plot) in indicated cochlear cells at P1 and P7, as determined by scqRT-PCR. Each circle represents an individual cell. White rectangles indicate means.
(G) scRT-PCR analyses of splicing of *Rest* exon 4 in indicated cochlear cells at P1 and P7.
(H) Quantification *Rest* exon 4 splicing in single cells from organ of Corti in P1 and P7 mice. Splicing is quantified as the percentage of *Rest* transcripts containing exon 4 versus total *Rest* transcripts. Values are mean ± SEM; n = 4 IHCs from 3 mice at P1, 4 IHCs from 2 mice at P7, 8 OHCs from 3 mice at P1, and 10 cells from 3 mice/group in other groups.
See also Figure S4.

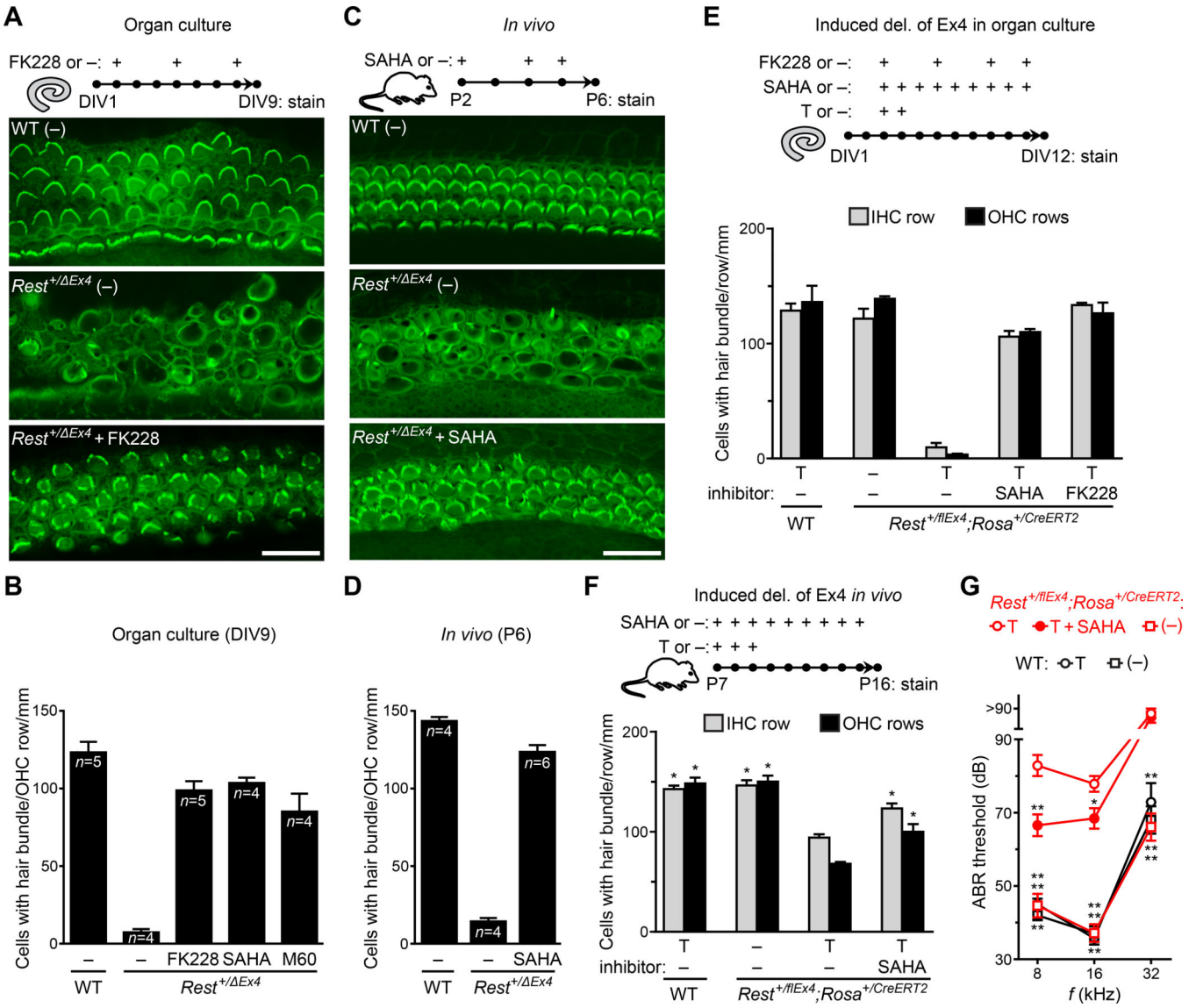

Figure 6. HDAC Inhibitors Rescue Hair Cells and Hearing of *Rest* Exon 4 Knockout Mice

(A) Effect of FK228 on OHC morphology in organ cultures from *Rest*$^{+/\Delta Ex4}$ mice. Top: schematic of treatment of organs of Corti from P1 *Rest*$^{+/\Delta Ex4}$ and WT mice is shown, from day *in vitro* 2 (DIV2) to DIV8 followed by visualization of F-actin on DIV9. Scale bar, 20 μm; solvent control, –.

(B) Numbers of cells with stereocilia bundles in OHC-containing regions of DIV9 organ of Corti cultures of the indicated genotypes and inhibitor treatments. Cultures were derived from P1 mice. Lack of stereocilia bundles served as indicator of OHC degeneration. Values are mean ± SEM; n, number of mice (1 culture/mouse/group).

(C) F-actin-stained preparations of organs of Corti from SAHA- or vehicle-treated *Rest* $^{+/\Delta Ex4}$ and WT mice at P6. Mice received SAHA or vehicle (–), as illustrated by the scheme at top. Scale bar, 20 μm.

(D) Numbers of OHCs with stereocilia bundles in middle turn of cochleas from *Rest*$^{+/\Delta Ex4}$ and WT mice at the end of treatment schedule depicted in (C). Values are mean ± SEM (n, number of mice).

(E) Numbers of hair cells with stereocilia bundles in DIV12 organ of Corti cultures derived from WT and *Rest*$^{+/flEx4}$;*Rosa*$^{+/CreERT2}$ mice at P5. Tamoxifen (T), SAHA, FK228, or solvent (–) was added at the indicated times. Values are mean ± SEM (n = 3 cultures from 3 mice/group).

(F) Numbers of hair cells with stereocilia bundles in the middle turn of the cochleas of WT and *Rest*$^{+/flEx4}$;*Rosa*$^{+/CreERT2}$ mice, at the end of the depicted treatment schedule. Values are mean ± SEM; n = 3 mice/group; two-way ANOVA, $p < 0.0001$; post hoc Dunnett's test, *$p \leq 0.003$, control group, *Rest*$^{+/flEx4}$;*Rosa*$^{+/CreERT2}$ + T.

(G) ABR thresholds of P16 WT and *Rest*$^{+/flEx4}$;*Rosa*$^{+/CreERT2}$ mice treated with tamoxifen (T), SAHA or vehicle, as indicated in (F). Values are mean ± SEM; n = 8 mice in T + SAHA group; 7 mice/group in other groups. Two-way ANOVA, $p < 0.0001$, post hoc Dunnett's test, *$p = 0.043$, **$p \leq 0.0002$; control group, *Rest*$^{+/flEx4}$;*Rosa*$^{+/CreERT2}$ + T.

See also Figures S5 and S6 and Table S5.